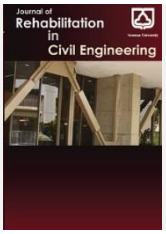

Journal of Rehabilitation in Civil Engineering

Journal homepage: https://civiljournal.semnan.ac.ir/

Study of the Effect of Soil-Pile-Structure Interaction on the Seismic Response of Steel Diagonal Grid Structures with Emphasis on Soil Liquefaction Phenomenon

Ebrahim Mirzaei [1]; Shahriar Tavousi Tafreshi [2,*]; and Farrokh Forootan [2]

1. Ph.D. Candidate, Department of Civil Engineering, CT.C., Islamic Azad University, Tehran, Iran
2. Assistant Professor, Department of Civil Engineering, CT.C., Islamic Azad University, Tehran, Iran
* Corresponding author: sh_tavousi@iauctb.ac.ir

ARTICLE INFO

Article history:
Received: 08 June 2025
Revised: 29 July 2025
Accepted: 17 August 2025

Keywords:
Soil-pile-structure interaction;
Diagonal grid steel structure;
Seismic response;
Liquefaction of soil.

ABSTRACT

The transition from internal frame structures to external systems like diagonal grids has enhanced both shear resistance and aesthetic value in tall buildings. These external systems effectively distribute load-bearing elements around the perimeter, utilizing triangular grid networks to optimize structural and architectural performance. However, a significant challenge in seismic regions is the liquefaction of loose sandy soils, which can cause severe settlement and lateral displacement. This research examines steel diagonal grid structures, focusing on soil-pile-structure interaction and liquefaction effects. A symmetric four-story model was developed using SAP2000 and modeled nonlinearly in OpenSees, incorporating near-field and far-field soil domains, piles, and structural elements. Results indicate that longer piles (28-30 meters) with diameters over 1.2 meters reduce roof displacement by up to 42%, while increasing shear forces and bending moments within the piles, maintaining foundation rotation within acceptable limits (less than 0.002 radians). In contrast, shorter piles (12 meters) decrease shear and axial forces but lead to increased roof displacement and inter-story drift, with increases up to 43%. Notably, under liquefaction, these shorter piles show a relative drift reduction of up to 62%. The findings stress the importance of a balanced design approach that considers both structural displacements and internal stresses, advocating for the integration of geotechnical and structural factors in seismic design for innovative systems like diagrids. Recommendations include refining design codes to impose specific limitations on pile dimensions to address nonlinear liquefaction effects.

E-ISSN: 2345-4423

How to cite this article:
Mirzaei, E., Tavousi Tafreshi, S. and Forootan, F. (2026). Study of the Effect of Soil-Pile-Structure Interaction on the Seismic Response of Steel Diagonal Grid Structures with Emphasis on Soil Liquefaction Phenomenon. Journal of Rehabilitation in Civil Engineering, 14(3), 2363 https://doi.org/10.22075/jrce.2025.2363

1. Introduction

The performance of buildings during earthquakes is influenced by various factors, including shape, size, force transmission to the ground, and the interaction between the structure and the underlying soil. Structures that are symmetrical and simpler in design tend to exhibit superior performance and lower vulnerability. Over time, structural systems have evolved from internal models to external models, such as diagonal grid systems, which enhance architectural aesthetics while providing necessary shear resistance.

Given the significant financial and human costs associated with earthquakes, studying soil-pile-structure interaction is crucial, particularly in regions with high seismic risk where soil liquefaction can compromise the performance of structures. Previous research has primarily focused on fixed structures, neglecting the mutual effects of soil and structure. A comprehensive understanding of this interaction, along with new analytical methods such as soil-pile-structure system modeling, is essential for mitigating earthquake-induced damages. Small-scale shaking table tests by Motamed et al. (2010) [1] investigated the behavior of various pile group configurations under lateral soil deformation. They concluded that thicker non-liquefied layers increase moment magnitude and that lateral soil pressure variations correlate well with soil displacement velocity, indicating fluid-like behavior of sand in liquefied states. Haeri et al. (2012) [2] explored deep foundation behavior due to lateral deformation using a shaking table device. Their findings indicated that increased pore water pressure leads to reduced acceleration amplitudes immediately after liquefaction, and that pore water pressure varies significantly around piles compared to the free field. They also noted that lateral soil pressure on piles is influenced by the position of the pile within the soil.

Mathematical modeling of soil-structure interaction involves complex differential equations, which can be time-consuming to solve accurately. In contrast, numerical modeling simplifies this by using algebraic equations, accommodating the complexities of material behavior, boundary conditions, and loading systems. Two primary methods are commonly employed to model piles under liquefaction phenomena: the nonlinear Winkler spring model and continuum analysis. In the nonlinear Winkler spring method, the pile is modeled as a beam, while surrounding soil is represented by linear springs for non-liquefied layers and nonlinear springs for liquefied layers. This method has been validated by various researchers, demonstrating reasonable accuracy compared to laboratory models. The continuum analysis method treats the pile and surrounding soil as a continuous medium, enabling the tracking of liquefaction mechanisms and solving coupled equations governing soil and pore fluid phases. Recent studies, such as those by Bagheri et al. (2018) [3], have evaluated the effects of seismic soil-pile-structure interaction (SSPSI) on the seismic responses of structures using numerical simulations. Their findings emphasize the importance of considering factors like pile lengths, diameters, spacings, and ground motion characteristics in the design of pile-raft foundations to enhance structural performance. López-Jiménez et al. (2018) [4] developed numerical models to analyze the performance of different foundation systems under seismic loading, finding that system type and excitation frequency significantly affect force distribution and displacement behavior. Brandis et al. (2022) [5] introduced a new methodology for soil-structure systems, demonstrating the feasibility of simplified displacement-based design methods. Mohaseb et al. (2020) [6] investigated the influence of soil-pile-structure interaction forces on the seismic response of tall building projects, revealing significant increases in fundamental vibration periods due to these interactions. Their work underscores the need for comprehensive seismic analyses that incorporate soil-structure interactions to ensure structural integrity during earthquakes. Konto Kuisp (2024) [7] proposed a low-cost, accurate approach for simulating pile-soil interaction, validating a coupled three-dimensional method that improves upon traditional modeling techniques. This method demonstrated high accuracy and efficiency in simulating the complex interactions between piles and soil.

The investigation into soil-pile-structure interaction (SPSI) and its influence on the seismic response of steel diagonal grid structures, particularly in the context of soil liquefaction, highlights significant insights into structural vulnerability during earthquakes. Liquefaction can cause severe ground displacements, adversely affecting structural stability, with buildings on liquefiable soils experiencing lateral spreading and substantial displacements [8]. Dynamic soil-structure interaction (SSI) analyses reveal that structures on such soils exhibit modified response spectra and displacements during seismic events [9]. Additionally, structure-soil-structure interaction (SSSI) effects are particularly pronounced in urban areas where multiple structures interact through the underlying soil, leading to amplified permanent tilt and settlement, especially with minimal spacing between buildings [10]. The nonlinear responses of structures under SSSI conditions differ markedly from those of isolated structures, underscoring the necessity for integrated design approaches [11]. Mitigation strategies, such as ground densification, have demonstrated the potential to reduce permanent settlement by up to 58% in liquefiable soils, although they may not effectively mitigate tilt in certain configurations [10]. Thus, a comprehensive understanding of SPSI and SSSI complexities is vital for developing effective mitigation strategies to enhance structural resilience against seismic hazards [12]. However, some studies indicate that the overall impact of SSSI may be less significant in specific configurations, suggesting a need for further research to fully comprehend these interactions in various urban environments.[11].

The present study aims to evaluate the seismic performance of steel braced frame structures considering soil-structure and pile interaction, particularly focusing on liquefaction effects. Using the beam-on-nonlinear-Winkler-foundation method, a four-story structural model will be analyzed and designed using SAP2000 software. The model's symmetric plan will facilitate the assessment of lateral and gravity loading results. Following foundation design, 2D models of the perimeter frame will be created in OpenSees software, connecting various components of the soil-pile-structure system. The applied modeling approach will be validated against results from centrifuge tests conducted by UC Davis. Nonlinear time history dynamic analysis will be performed, with outputs processed to evaluate the effects of liquefaction on structural responses.

2. Research significance

Given that Iran is located in a highly seismic region and that surface soils at construction sites often consist of loose or semi-dense sandy layers, there is a possibility of soil liquefaction occurring. Considering the critical importance of diagrid structures, the nature of the loads applied to them, and the inclined columns they contain, the structural members and piles in such systems are typically designed with sufficient stiffness and strength to ensure their integrity. As a result, notable nonlinear behavior in these structures generally occurs only in areas of very high seismicity and under exceptional conditions, such as global instability due to seismic loading.

The main objective of this research is to examine the process of liquefaction's phenomenon effects on the seismic response of diagrid structures using a practical finite element model. In this research, to achieve this objective, all analyses are performed in both conditions of liquefaction occurrence and non-occurrence, so that by comparing these two conditions, the mechanisms and influencing processes of this phenomenon on the seismic behavior of diagrid structures are revealed. This topic has not been observed in the technical literature to date, and the results of this research can provide designers with good insight into the foundation design of diagrid structures and even the structure itself. Structural characteristics such as stiffness, structural form, structural height, and structural efforts can be considered influential parameters in inertial interaction (overall system interaction). On the other hand, in liquefied and non-liquefied sandy soil conditions, structural responses change, and the investigation of this topic has also not been studied to date.

3. Materials and methods

This research employs OpenSees – an open-source, object-oriented finite element framework developed at UC Berkeley by Frank et al. (2000) [13] – for nonlinear modeling and analysis of soil-pile-structure systems. Widely recognized as a powerful tool in earthquake engineering, OpenSees utilizes behavioral models based on stress-strain responses to define material properties, forming the core of numerical simulations. The study implements the Beam on Nonlinear Winkler Foundation (BNWF) method, structured in three components:

1. Pile and structure elements
2. Free-field soil elements (representing far-field conditions)
3. Near-field elements connecting the pile to the surrounding soil column.

These elements collectively model soil-structure interaction under seismic loading. The paper subsequently details the specific material and element behavioral models used in this framework to capture system nonlinearity.

3.1. Steel material behavioral model

Materials used for beam and inclined column members of diagrid structures are steel type. For defining steel materials, Steel02 materials available in the OpenSees software library [13] have been used.

3.2. Concrete material behavioral model

Materials used for foundation pile members are concrete type. For defining concrete materials, Concrete02 materials available in the OpenSees software library have been used [13].

3.3. Far-field sandy soil behavioral model

This research emphasizes the critical selection of a sand behavioral model that accurately captures saturated sand characteristics—including initial shear stress, confining pressure, and density—under seismic loading. The study employs the PressureDependMultiYield02 material from OpenSees, an elastoplastic model based on Prevost's (1985) multi-surface framework [14] and modified by Elgamal et al. (2003) [15,16] to simulate liquefaction. This model replicates pressure-sensitive soil behavior, volume changes during shear, and liquefaction in sands/silts under cyclic loading. The parameters selected for defining PressureDependMultiYield02 material in OpenSees were adopted from reference [17].

To accommodate both liquefiable and non-liquefiable sandy soil conditions, key adjustments were made for non-liquefiable scenarios: (1) assuming high permeability (1 m/s) for full drainage, and (2) setting all contraction/dilation parameters to zero. This prevents excess pore pressure buildup while preserving calibrated shear modulus and damping properties [18].

3.4. Constitutive model for near-field sandy and clayey soils (interaction zone)

To model the pile-soil-structure interaction zone, two sets of springs are used: lateral and axial springs. This section introduces these springs.

3.4.1. Lateral springs

In this study, the PyLiq1 lateral spring (an uniaxial material) is used for modeling the liquefaction effects. This material, utilized a zero-length element, connects the two-dimensional plane strain soil mesh to pile elements. In conditions where excess pore water pressure does not exist, such as gravity loading, the behavior of this material is similar to conventional P-y curves; therefore, the fundamental equations governing this material are the same as conventional p-y curves. This material has two modeling modes: in the first mode, the behavior is elastic and independent of any excess pore water pressure in specified adjacent soil elements. In the second mode, after updating the state of this material, the material's

behavior is generally consistent with undrained loading and susceptibility to pore water pressure increase. Two soil elements above and below its position are assigned to the zero-length element of this material. The rate of pore water pressure increase in soil elements is calculated according to equation (1):

$$r_u = 1 - \frac{p'}{p'_c} \quad (1)$$

The pore pressure ratio (r_u) is calculated using mean effective stresses: p'_c (pre-consolidation stress) and p' (current mean effective stress) from two assigned soil elements. The average ruru from these elements scales the PyLiq1 spring's ultimate resistance and initial stiffness via the factor ($1-r_u$), reducing stiffness/resistance as pore pressure rises during dynamic analysis. However, resistance cannot drop below a minimum residual value—here set to 10% of the spring's original ultimate resistance to represent liquefied soil behavior. This ensures realistic modeling of strength loss while preventing unphysical zero-resistance conditions.

3.4.2. Axial springs

To model the soil behavior under axial loads, a combination of uniaxial materials and zero-length elements is used. Two types of uniaxial materials are employed in this study for modeling axial springs:

1. TzLiq1 material: used to simulate shaft resistance and soil behavior under axial loading in the presence of liquefaction.
2. QzSimple1 material: used to simulate the end-bearing resistance of the pile.

It is worth mentioning that the TzLiq1 material is a uniaxial material based on the conventional t-z curves and considers liquefaction effects similar to the PyLiq1 lateral spring. API (American Petroleum Institute) [19] code recommendations are used for assigning the properties of the p-y, t-z, and q-z springs.

3.5. Element types used in modeling

The elements used to model the pile-soil-structure interaction system include:

1. Nonlinear beam-column elements for the inclined column members of the steel braced frame structure.
2. Elastic beam-column elements for the beam members of the same structure.
3. Zero-length elements to define Winkler springs in the interaction zone.
4. 9-node quadrilateral plane strain elements for the soil domain.

4. Validation of the soil-pile-structure interaction model

Laboratory test results by Wilson [18] at the University of California, Davis (UC Davis) were used to validate the soil-pile-structure interaction model using the single-stage beam-on-nonlinear-Winkler foundation (BNWF) approach. Five cases of the experiments are made with respect to the type of soil and input motion records.

1. CSP1 group: There are two sand layers in the soil with pore fluid of water. The upper layer has a relative density of 55%, is 1.6 m thick and the lower layer has a relative density of 80%, 11.4 m thick.
2. CSP2 group: The upper layer (1.6 m) has a relative density between 35–40%, and the lower layer (11.4 m) has an 80% relative density. The low density of the surface sand leads to a high potential for liquefaction.
3. CSP3 group: Includes models with an upper sand layer of 55% relative density and a lower sand layer of 80% with pore fluid of a mixture of water and hydroxy-propyl methylcellulose (HPMC).
4. CSP4 and CSP5 groups: The upper layer (1.6 m) consists of normally consolidated clay, while the lower layer is sand with an 80% relative density.

The results of these experiments, along with all related data, are publicly available on the university's website (https://www.ucdavis.edu/research/labs-to-lives). It is noteworthy that the experimental results were scaled to full prototype dimensions and presented in the form of reports. Therefore, for the finite element modeling, the scaled-up real dimensions of the soil-pile-structure system were used instead of their centrifuge model counterparts. The centrifuge device at UC Davis was a 9-meter radius device that can generate gravitational acceleration up to 30g. All of these experiments use the uniform and fine Nevada Sand.

4.1. Experimental description

To evaluate the finite element model presented in the subsequent section, the results of the CSP2 experiment have been utilized. The soil profile in this experiment consists of two horizontal soil layers. Nevada sand with a relative density of 80 percent is in the lower layer and loose Nevada sand with a relative density of 35 percent is in the upper layer. The steel tubular pile to be analyzed has a diameter of 0.67 m, a length of 20.6 m, a wall thickness of 19 mm, and a flexural rigidity of 417 MN.m^2. Figure 1 illustrates the overall view of soil stratification in this experiment. The concentrated mass at the top of the pile is approximately 500 kN, with its height from ground surface being approximately 6 times the pile diameter. The specifications of the soil employed in this experiment are presented in Table 1.

It is important to note that the continuum model was developed using OpenSees, an open-source, object-oriented finite element analysis framework [20]. To visualize the finite element mesh, the GiD software was employed [21]. OpenSees offers robust capabilities for earthquake engineering simulations by integrating advanced models for both structural and geotechnical components, enabling comprehensive analysis of soil-structure interaction and seismic response.

Table 1. Characteristics of Sandy Soil Utilized in Wilson's Experiments [18].

Soil Type	Internal Friction Angle (φ°)	Buoyant Unit Weight γ' (KN/m³)
Sand with 35% compaction	30	9.8
Sand with 80% compaction	40	10.1

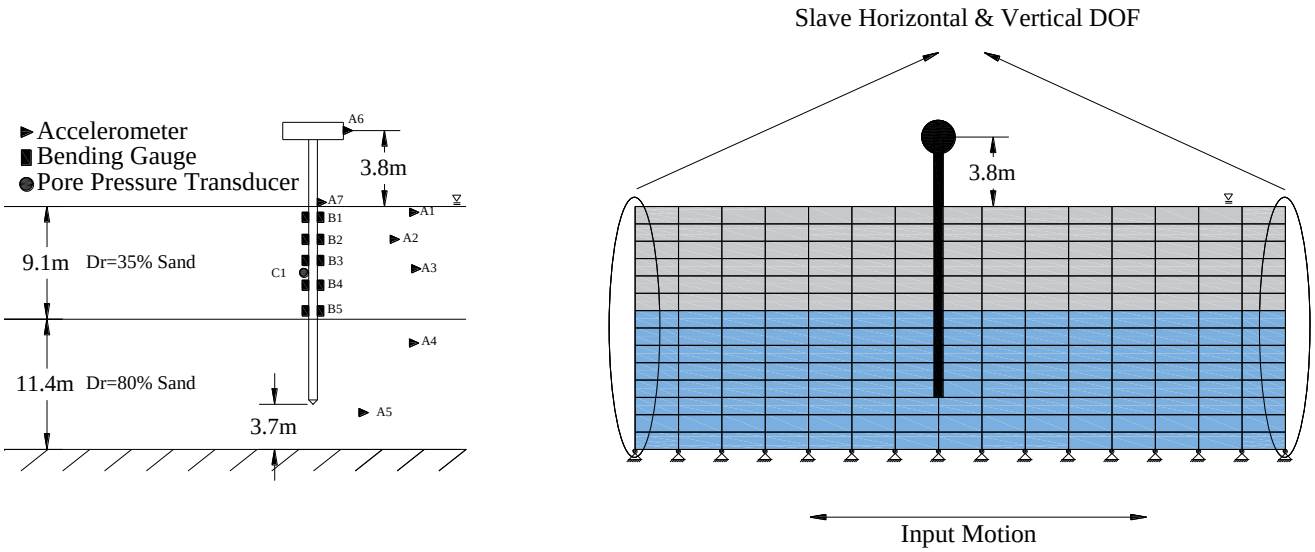

Fig. 1. General Schematic of Test Configuration and Its Finite Element Model [18].

In these experiments, earthquake records from Kobe recorded by a station in Port Island and the Loma Prieta earthquake record captured by the UCSC station in Santa Cruz were employed. The recorded data

at the bottom of the soil column was utilized as input ground motion, and the modeling of the apparatus container and its effects on the dynamic response of soil was neglected [22].

4.2. Description of the finite element model using single-stage beam-on-nonlinear-winkler-foundation approach

The finite element model presented in this research encompasses soil elements to capture far-field soil response, nonlinear beam elements for structural components, and connecting soil springs to link the far-field soil to pile elements. A two dimensional plane strain model was used for nonlinear time-history analysis of pile-soil system using OpenSees software. In the previous section, the materials and elements used in the finite element model were introduced.

4.3. Damping

The conventional method of Rayleigh damping coefficients was used for material damping assignment. In order to solve the problem, the solution domain was subdivided into structure and soil regions, with the coefficients for each region applied separately. It is noteworthy that in the soil region, considering that in the elastoplastic behavioral model of El-Gamal, a significant percentage of energy is dissipated through hysteretic damping (resulting from inelastic soil behavior), only a small amount of Rayleigh damping is applied to the soil mesh for numerical solution stability and damping at very small strains ([17,23]). Additionally, radiation damping is obtained using coefficients proposed by Berger from the equation (2):

$$c_L = 4D\rho V_s \tag{2}$$

Where c_L represents the soil radiation damping coefficient, D denotes pile diameter, ρ is soil density, and V_s represents shear wave velocity in soil.

4.4. Boundary conditions in two-dimensional soil mesh

A uniform excitation command is used, and the nodes on the bottom end of soil column constrain the two translational degrees of freedom of soil elements. This assumption indicates that all seismic wave energy is dissipated within the soil medium. Given the significantly higher stiffness of the container relative to the soil within it, this assumption appears reasonable [22]. Soil nodes at identical elevations on both lateral boundaries of the soil mesh are tied together in their translational degrees of freedom. Assuming this, only shear waves are propagated through the soil column. The out-of-plane thickness of soil elements is considered very large. Consequently, the weight of soil elements becomes substantially large to prevent the kinematic effects of the pile on the two-dimensional soil mesh, which is intended to model only far-field soil behavior. It should be noted that increasing the out-of-plane thickness of soil elements has no effect on shear wave propagation in the soil medium and is employed solely to maintain the plane strain condition of the far-field soil medium ([17,23,24]). Figure 2 illustrates the correct pattern of shear wave propagation and soil column deformation.

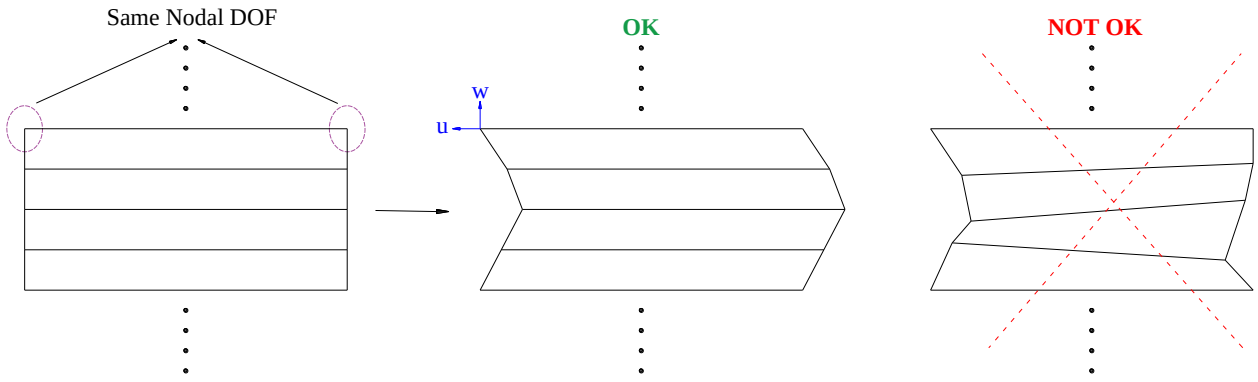

Fig. 2. Correct Pattern of Shear Wave Propagation and Soil Column Displacement [25].

The soil member's height is proportional to the shear wavelength of the softest layer. The shortest wavelength of the shear wave must be captured by at least 4 elements across the shortest wavelength of the shear wave throughout the soil mesh. Equation (3) [25] is used to determine the maximum height of the soil elements.

$$h_{max} = \frac{v_s}{8 f_{max}} \tag{3}$$

Where h_{max} represents maximum height in meters, f_{max} denotes maximum frequency content of input ground motions, and V_s represents shear wave velocity in meters per second in the softest soil layer. Assuming that the maximum frequency content of ground motion is conservatively 40 Hz and the shear wave velocity in the sand layer with 35% relative density equals 160 m/s, using the above equation, the maximum height of soil elements is determined to be 0.5 meters [26].

4.5. Modeling approach for soil-pile-structure interaction in single-stage beam-on-nonlinear-winkler-foundation method

Direct connection of two-dimensional soil mesh nodes to nonlinear beam element nodes of the pile through soil springs results in the generation of artificial forces in the pile ([17][23,25]). The reason for this phenomenon is that following gravitational loading in the two-dimensional mesh, the soil undergoes settlement. Consequently, artificial forces are generated in the springs and subsequently in the piles. However, in reality, it is assumed that this soil settlement occurs over an extended period, and the pile is installed after this settlement has taken place. Furthermore, occasionally, due to soil meshing and the coordinates of pile element nodes, a relative distance is created between pile nodes and the nearest point of the two-dimensional soil mesh. This issue becomes more pronounced in inclined piles and regular square two-dimensional meshes. Therefore, in such cases, zero-length elements cannot be employed to connect these nodes with different coordinates.

Consequently, considering the aforementioned reasons, this research employs the method of defining fictitious nodes at identical coordinates with the nearest point of the two-dimensional soil mesh, which is a feature of OpenSees software. Fictitious nodes are defined in two dimensions with three translational degrees of freedom and coordinates identical to the nearest soil mesh nodes to pile nodes. These nodes are constrained in their rotational degree of freedom, as their function is to apply vertical and horizontal displacements of the two-dimensional soil mesh through Winkler springs to pile elements, and no rotation should be applied to these nodes during analysis due to the inertia of structural members.

The finite element model is unstable if the rotational degree of freedom in these nodes is not constrained. The fictitious nodes at the same coordinate are connected to the two-dimensional soil mesh nodes by zero-length elements, which establishes soil springs.

After the soil is gravitationally loaded, the fictitious nodes connected to the beam-column element nodes of the pile in the translational degrees of freedom in the horizontal and vertical directions. Consequently, through this technique, gravitational displacements of the soil medium are not transferred to the interaction zone and structure, preventing the generation of artificial forces. These same fictitious nodes are utilized for defining other soil springs as well. Figure 3 presents the configuration of this method for horizontal soil springs.

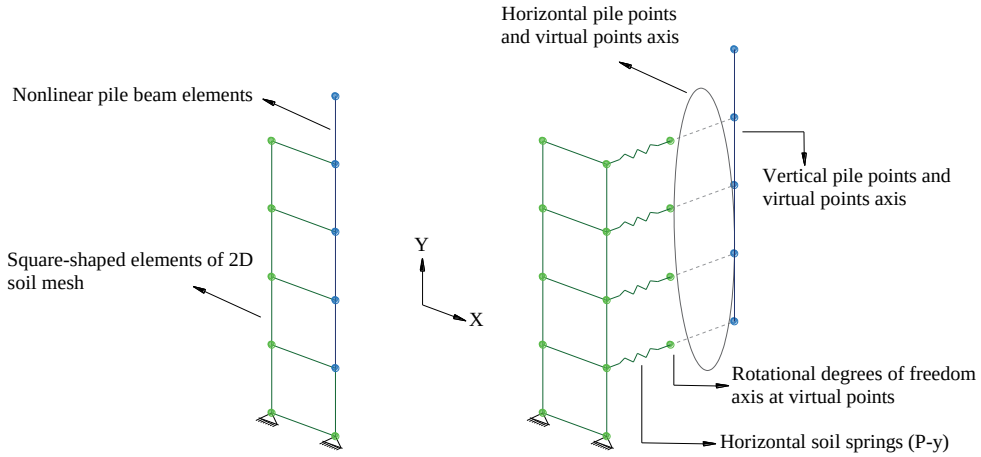

Fig. 3. General Configuration of Connection Between Pile Nodes and Two-Dimensional Soil Mesh in Overall and Expanded Views.

4.6. Solution method

During the application of dead gravitational loads of soil and structure, large numerical damping and large time intervals were employed. By assigning this large numerical damping, the nonlinear transient analysis simulates quasi-static loading conditions [27]. Therefore, during the application of dead loads of soil and structure, the analysis procedure becomes highly damped through the assignment of values 1.5 and 1.0 for Newmark time integration parameters β and γ, respectively. Dynamic analyses were performed using transient analysis with variable time steps and Newmark integrator (average acceleration method). Transient analysis with variable time steps automatically reduces the time step in case of solution non-convergence. It should be noted that transient analyses were utilized in both gravitational load and dynamic load analysis phases. The reason for this approach is to prevent numerical solution problems arising from the simultaneous use of static and transient analyses in pile-soil-structure system modeling.

4.7. Analysis phases

Failure to strictly observe modeling considerations results in the generation of undesirable and unrealistic artificial stresses in piles. This section enumerates the various analysis phases and describes the procedure for preventing unrealistic artificial forces in piles. The analysis phases consist of:

1. In this phase, the geometry of the finite element model is defined. This phase includes the geometry of the soil column, pile, and fictitious nodes. In defining nonlinear beam-column elements for the pile, several fiber elements are assigned. Nonlinear soil springs are created and defined between two-dimensional soil mesh nodes and fictitious nodes established at identical coordinates through zero-length elements. In this phase, fictitious nodes are not tied to pile nodes.
2. In this phase, an elastic gravitational analysis is employed to simulate subsurface conditions. This phase is conducted as a transient analysis with very large time intervals to obtain correct hydrostatic pore water pressure states.
3. The soil material state is updated to a nonlinear condition, and several transient dynamic analyses are applied for initial value adaptation. For better convergence of these phases, they are performed with smaller time intervals.
4. In this phase, fictitious soil nodes and pile element nodes are tied together. Tying pile nodes to fictitious nodes at this stage prevents the generation of artificial forces, as the structural system did not participate in the gravitational load analysis of the two-dimensional soil mesh, and displacements resulting from soil settlement are not unrealistically applied to soil springs and

structures. Several phases of transient analysis are performed for dead load application of the structure.

5. In this phase, the state of PyLiq1 and TzLiq1 materials is updated. These materials consider the average effective stress of two soil elements assigned to them as initial consolidation stress before undrained loading. From this phase onward and throughout the entire time-history analysis, the behavior of these materials will be dependent on the effective stresses of the medium and pore water pressures.
6. In the final phase, transient time-history analysis with variable time steps is employed for seismic analysis of the pile-soil-structure system finite element model.

4.8. Comparison of laboratory and finite element model results

To evaluate the soil-pile-structure system finite element model, computed dynamic responses were compared with recorded results from centrifuge experiments. Response comparisons were conducted in two general groups. The first group examined the accuracy of the far-field soil model, including elastic response spectra of soil at various depths and the trend of pore water pressure increase in the two-dimensional soil mesh. The second group investigated computed responses in the structure, such as superstructure acceleration time histories, superstructure elastic response spectra, superstructure horizontal displacement time histories, and maximum moments generated in the pile at various depths.

Figures 4 through 7 respectively compare soil elastic response spectra at the ground surface, at depths of 7.44 meters, 10.7 meters, and 13.9 meters. Figures 8 and 9 show comparisons of pore water pressure increase trends at depths of 3.5 meters and 7.5 meters, respectively. Furthermore, Figure 10 compares acceleration time histories in the superstructure, Figure 11 compares superstructure elastic response spectra, Figure 12 compares recorded displacement time histories in the superstructure, and Figure 13 compares maximum bending moments at various depths.

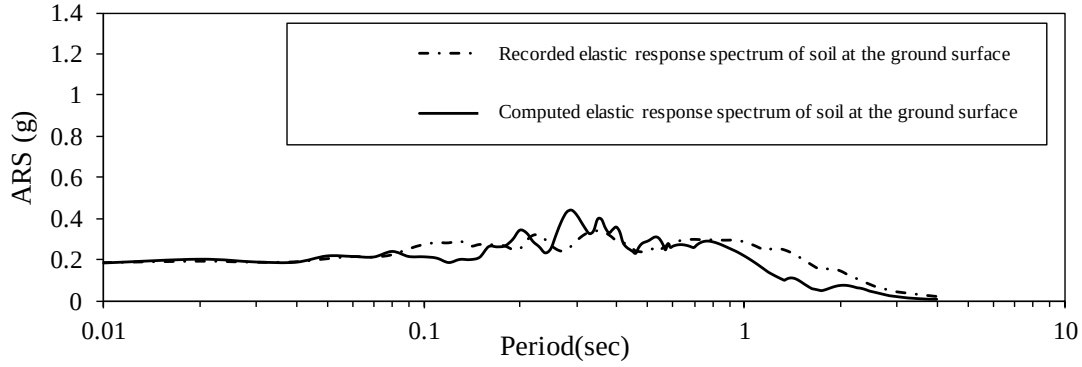

Fig. 4. Comparison of Soil Elastic Response Spectrum at Ground Surface.

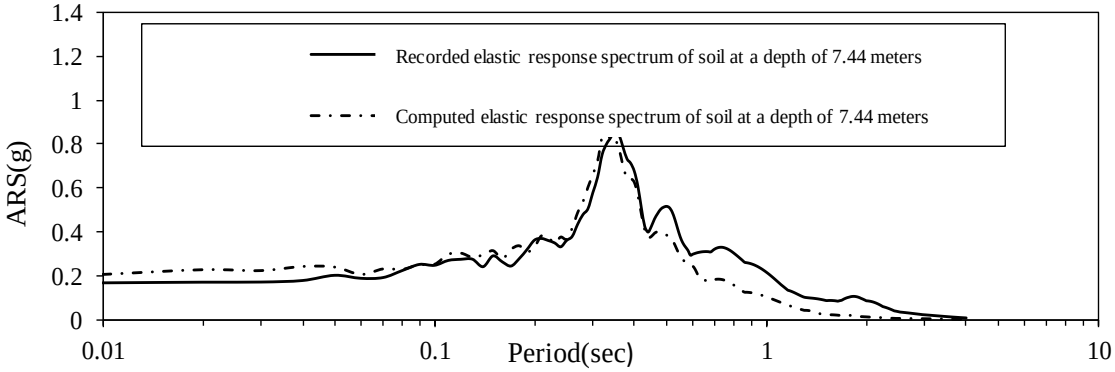

Fig. 5. Comparison of Soil Elastic Response Spectrum at 7.44-meter Depth.

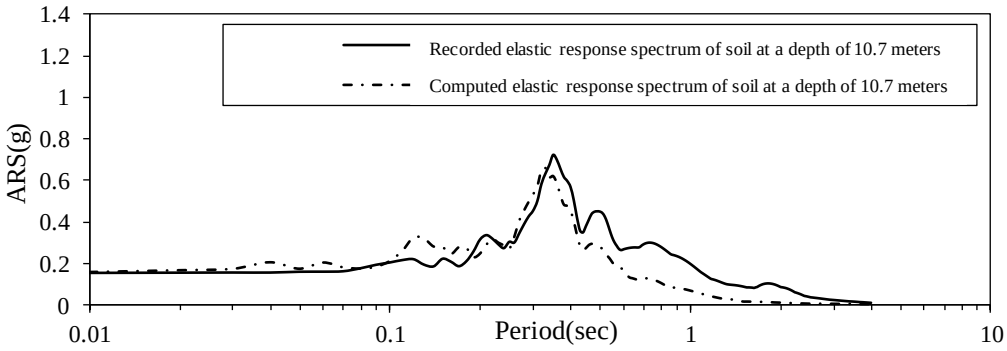

Fig. 6. Comparison of Soil Elastic Response Spectrum at 10.7-meter Depth.

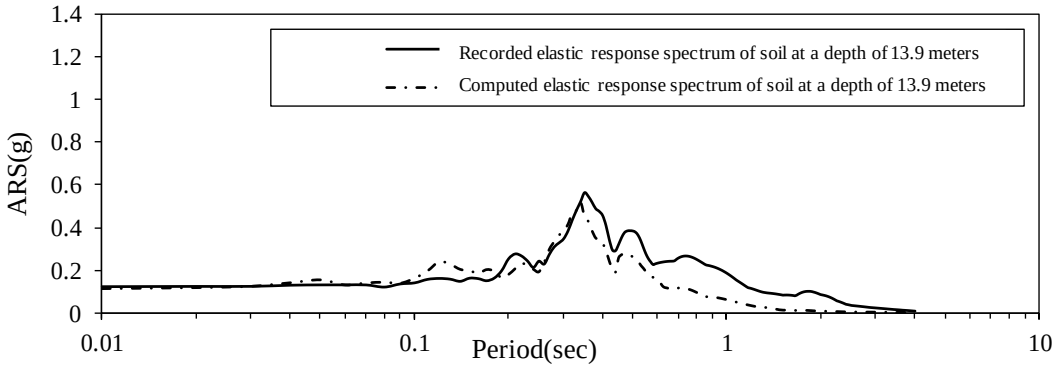

Fig. 7. Comparison of Soil Elastic Response Spectrum at 13.9-meter Depth.

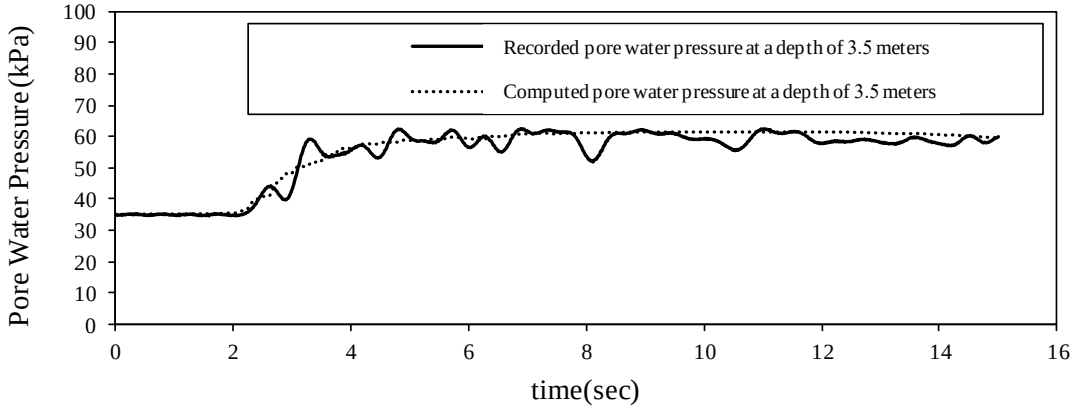

Fig. 8. Comparison of Pore Water Pressure Increase Trend at 3.5-meter Depth.

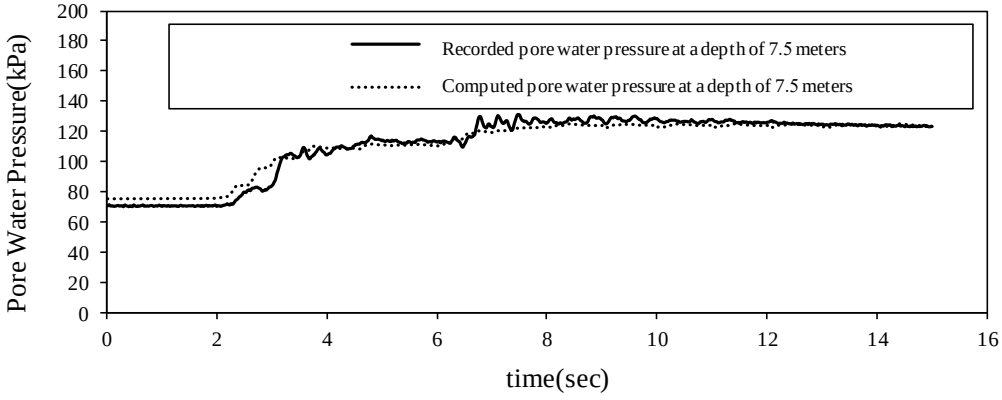

Fig. 9. Comparison of Pore Water Pressure Increase Trend at 7.5-meter Depth.

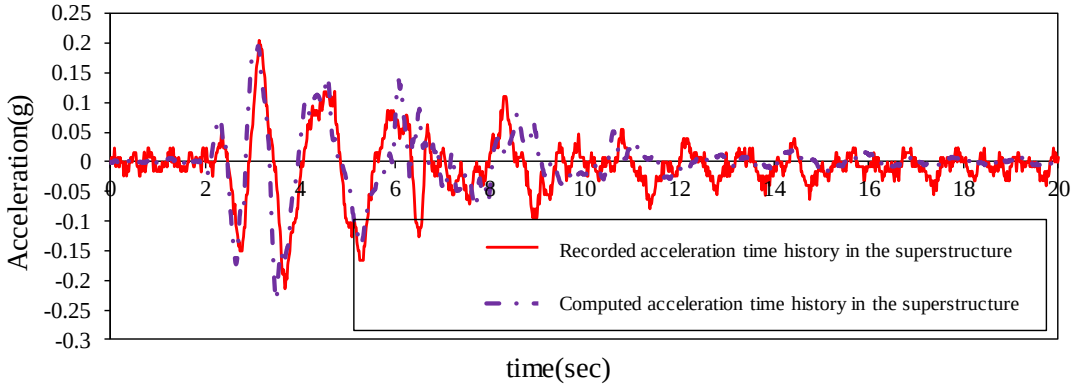

Fig. 10. Comparison of Acceleration Time History in Superstructure.

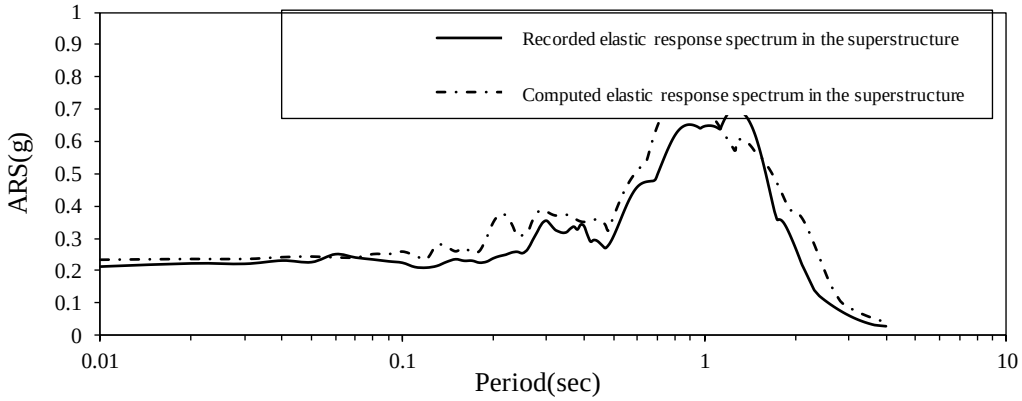

Fig. 11. Comparison of Superstructure Elastic Response Spectrum.

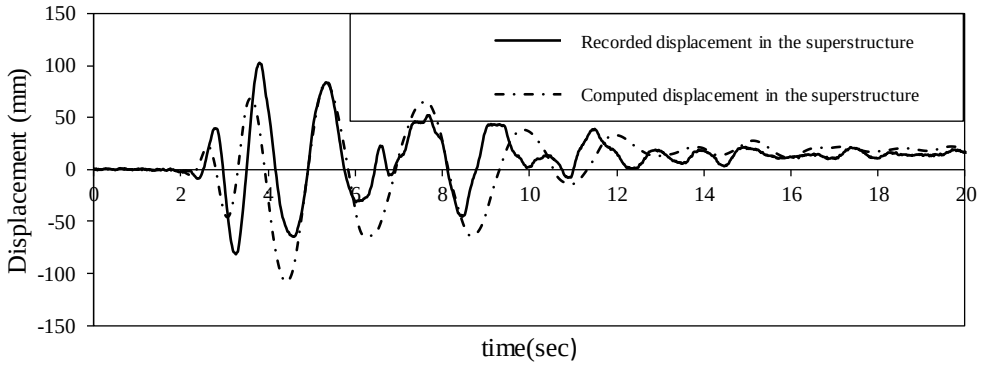

Fig. 12. Comparison of Recorded Displacement Time Histories in Superstructure.

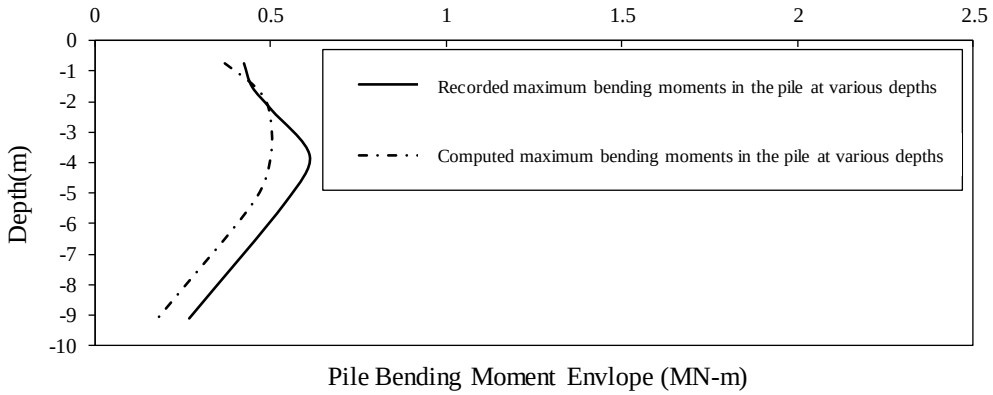

Fig. 13. Comparison of Maximum Pile Bending Moment at Various Depths.

Except for the soil elastic response spectrum at ground level—which shows a notable 24% difference—the recorded maximum spectral acceleration values exhibit only minor discrepancies (ranging from 3% to 9%). This indicates a high degree of accuracy in the numerical model. The larger deviation observed at the ground surface may be attributed to the exclusion of the apparatus container and its stiffness in the model. This issue was previously examined by Ilankatharan [22], who modeled the soil-pile-structure interaction under two conditions: (1) soil alone, and (2) soil with the apparatus container. He concluded that omitting the container leads to a slightly greater difference between the finite element model and laboratory results for the soil elastic response spectrum at the ground surface.

An important observation is that elastic response spectra tend to increase with depth, a behavior driven by soil amplification effects. However, at the ground surface, the soil elastic response spectrum decreases compared to lower layers. This reduction is due to increased pore water pressure and the onset of liquefaction, which causes the upper soil layer to behave like a highly viscous fluid. This fluid-like behavior inhibits shear wave propagation, thereby lowering the spectral acceleration values.

The predicted pore water pressure peaks show a close match with laboratory measurements, differing by only 1.6% to 2.2%. Similarly, the numerical model demonstrates strong accuracy in capturing superstructure acceleration time histories and elastic response spectra, with a peak difference of just 5%. As shown in Figure 12, the finite element model effectively captures both permanent and maximum displacements in the superstructure, with a 9% peak difference. However, a relative phase shift is observed between the displacement trends in the model and laboratory data, likely due to numerical simulation errors.

Based on its proven accuracy, practical applicability, and computational efficiency, this study employs a single-stage beam-on-nonlinear Winkler foundation modeling approach to simulate the diagrid structure.

5. Steel diagrid structure modeling

According to the research of Heshmati and Aghakouchak, 2019 [28], an angle between 60 to 70 degrees for inclined columns of diagrid structures can be effective in improving seismic responses and reducing steel consumption. Diagrid structures with a diagonal angle of 67º have demonstrated the ability to minimize steel material consumption while offering sufficient stiffness to withstand lateral loading. Therefore, a slope of 67º stands out as the most optimal choice for the design, leading to the exclusion of other slopes from consideration in this study. Story height is 3.5 meters, and column spacing is 6 meters. The studied plan and frame are shown in Figures 14 and 15, respectively. It should be noted that dead load, live load, and floor partition values are 550, 300, and 150 kg/m², respectively [29].

Additionally, steel yield stress of 240,000 kN/m², ultimate stress of 370,000 kN/m², and elastic modulus of 2.1E+8 kN/m² were considered [30,31]. The response modification factor in this study was assumed to be 4.5 [29]. The properties of the sections of each member is provided according to Table 2. The considered sections are seismically compact according to Table I-8-1 of the AISC 341-10 code [30]. Design criteria for beams, columns, and diagonal members were used based on AISC 360-10 code [31].

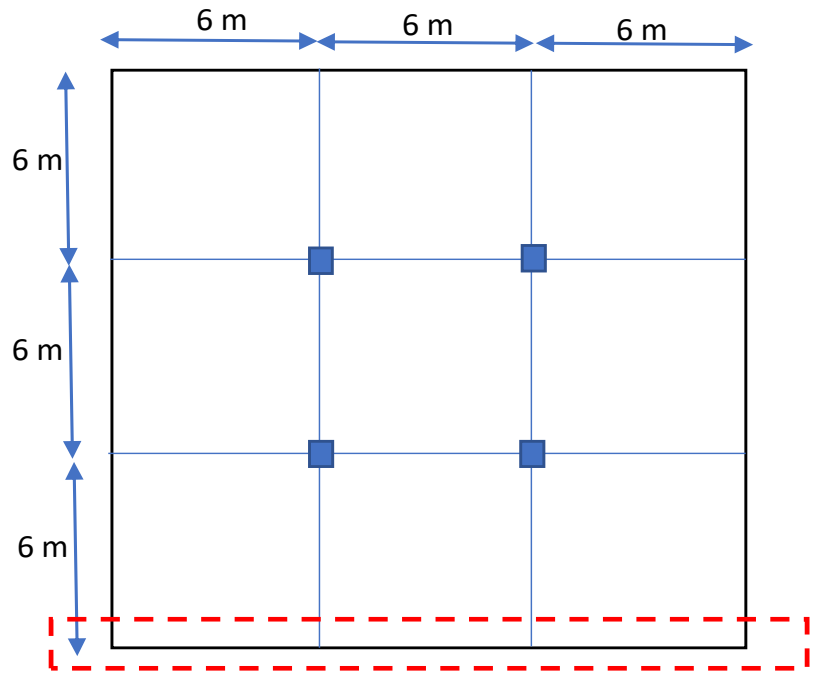

Fig. 14. Plan and Frame Under Study.

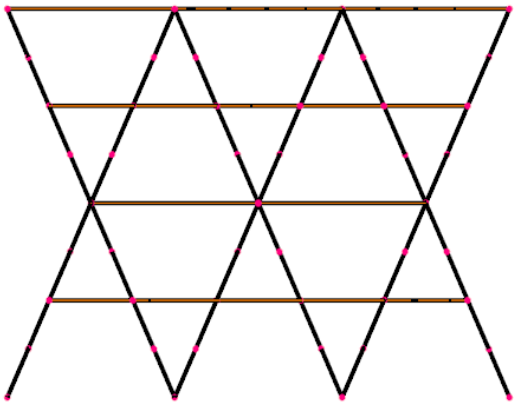

Fig. 15. 4-Story Frame Under Study.

Table 2. The properties of steel sections.

Story Number	Beam	Diagonal Members
1-4	IPE 200	Tube 450×20 mm

In this study, for the diagonal members of the braced frame system, beam-column elements with concentrated hinges were employed. This element idealizes plasticity as occurring within a defined hinge region, rather than being distributed throughout the entire member. Through this approach, the member is divided into three segments: two plastic hinges at the extremities and an elastic region in the middle. The plastic hinge length in this study was considered to be 100 centimeters. Figure 16 illustrates the specifications of the beam-column element with the concentrated hinge. The structural beams were modeled using linear beam-column elements. For transferring stiffness and resistance forces from local coordinate systems to global coordinates, corotational geometric transformation was utilized. This command is employed to construct a corotational transformation that transfers the element's stiffness and resistance forces under precise geometric transformation from the local coordinate system to global coordinates [13]. This transformation is used to account for the effects of large deformations and small

strains. Through the implementation of this transformation, geometric nonlinear behavior was incorporated.

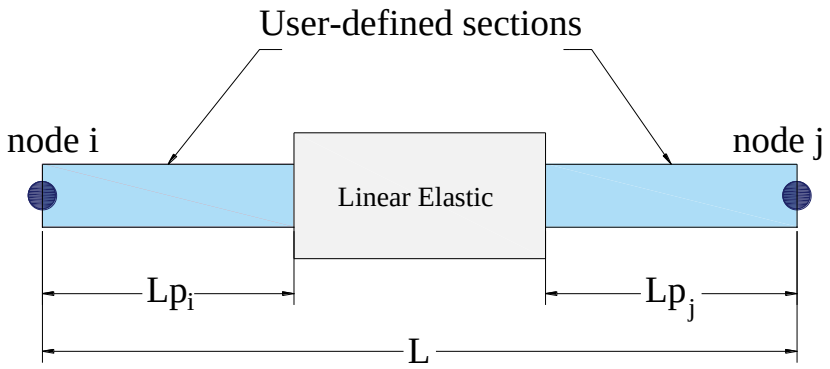

Fig. 16. Schematic representation of beam-column element with concentrated hinge [13].

Local or global buckling is the usual experience of steel members. Since seismic compactness criteria were considered in the section selection during the design process the likelihood of local buckling in sections is very low can be neglected. Consequently, diagonal members in these structures may experience global buckling. In this research, for modeling global buckling in these members, the Uriz and Mahin report was utilized. Figure 17 demonstrates the cyclic response of a bracing member with a tubular cross-section. This experiment was conducted by Black, the details of which are comprehensively presented in the Uriz and Mahin report. As illustrated in the figure, in the compressive region, the member's compressive capacity diminishes in successive cycles due to buckling. In this study, the aforementioned experiment served as the benchmark for buckling validation. For modeling diagonal members and incorporating their buckling effects in OpenSees software, the introduction of geometric imperfection along the brace length was employed. Figure 17 presents the modeling details in the software, and cyclic loading was applied according to the figure. As observed in Figure 18, excellent agreement between results is demonstrated.

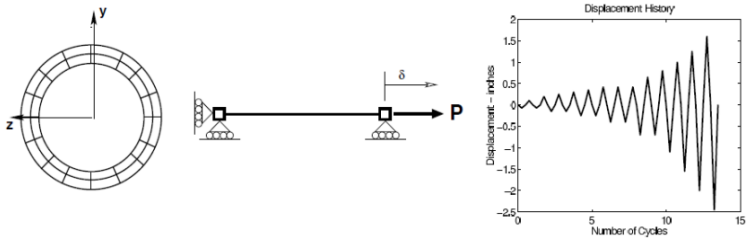

Fig. 17. Details of Black's experiment modeling in software.

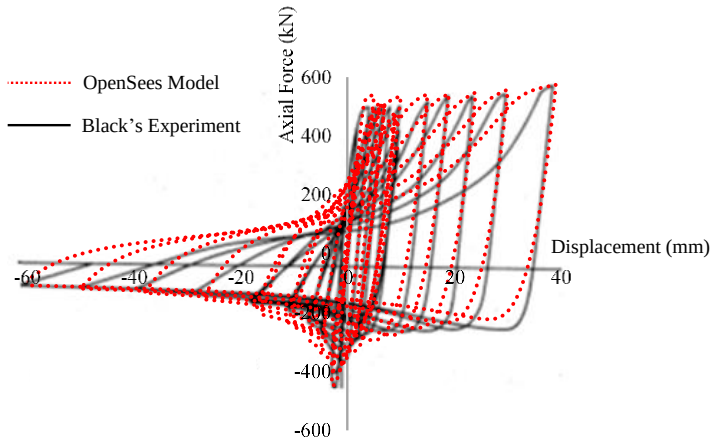

Fig. 18. Correspondence between experimental results and modeling.

6. Ground motion records utilized

In this study, an effort was made to consider a wide range of frequency contents in the selected records. The selection of records is based on Eurocode 8 for ground type A (rock or rock-like geological formations with Vs,30>800 m/s, as defined in Eurocode 8). According to the code's guidelines, the minimum prescribed duration of strong ground motion (D5–D95) is 10 seconds. Accordingly, a suite of seven ground motion records was employed for use in nonlinear dynamic analyses. Table 3 provides supplementary specifications of these ground motion records. Input excitation, similar to shear waves, was applied to the lowest level of the numerical model (model base) and propagated vertically through the soil volume. Furthermore, these records were filtered in SeismoSignal software within the 0.1 to 15 Hz range to focus on frequencies relevant for seismic signal analysis. This range captures essential seismic wave characteristics and eliminates noise, ensuring an accurate reflection of the seismic response during earthquakes. Figure 19 shows the standard spectrum and average of the seven records utilized. The significance of the average spectrum is that it consolidates the frequency content from the seven records, revealing common characteristics and trends that individual records may not show. This averaging enhances the reliability of the findings and aids in understanding the overall seismic response, facilitating comparisons with other studies. The ground motion records were scaled in the range of 0.2 to 1.5 times [32] the fundamental period to simulate a realistic range of seismic responses for structures, allowing for the evaluation of their performance under varying intensities of ground shaking. This approach helps in understanding structural behavior and informs more robust design recommendations. It is noteworthy that the mean elastic response spectrum of these records exhibits a close similarity to the response spectrum of ground type A [32].

Table 3. Specifications of ground motion records utilized.

Earthquake	Station	Year	Country	PGA (g)	Arias Intensity (m/s)	D5-D95 (sec)
Taiwan SMART	SMART1 E02	1986	China	0.142	0.794	12.31
Iwate	Minase Yuzawa	2008	Japan	0.205	0.981	10.79
Chi Chi	TCU138	1999	China	0.122	1.135	10
Darfield	LPCC	2010	New Zealand	0.228	1.751	12.06
Chuetsu-oki	Joetsu Uragawaraku Kamabucchi	2007	Japan	0.24	0.754	12.43
Loma Prieta	San Jose - Santa Teresa Hills	1989	USA	0.254	0.881	10.09
Hector Mine	Hector	1999	USA	0.264	1.212	11.62

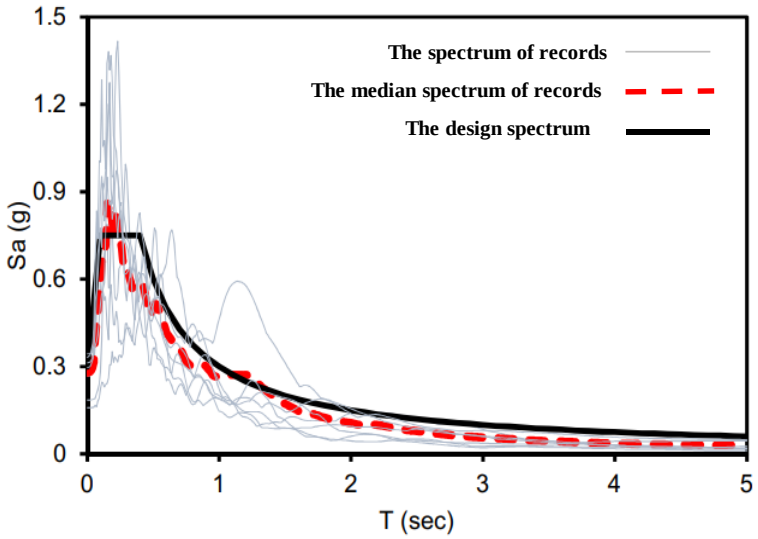

Fig. 19. Ground motion records spectrum.

7. Soil stratification employed for considering liquefaction effects

The soil layers comprise two sandy soil layers with different stiffness. Given the primary objective of this research, it is necessary to modify the soil stratification, particularly near the ground surface, to sandy soil. In this research, the maximum depth of the liquefaction phenomenon occurrence was selected as 8 meters, since below 8-meters depth, the probability of complete occurrence of this phenomenon decreases [33]. Consequently, the maximum thickness of the liquefiable layer in this research was considered to be 8 meters. Additionally, considering that in coastal areas, lands reclaimed from the sea and coastal regions generally have a loose sand layer over a dense layer, in the stratification selected for this research, a dense sand layer extending to 22-meters depth was also placed beneath it. The specifications of soil layers and their arrangement are presented in Table 4 and Figure 20, respectively.

Table 4. Soil layer specifications [17].

Description	Unit	Dense Sand	Liquefiable Sand	Parameter
Standard Penetration Test Number	-	35	15	$(N_1)_{60}$
Relative Density Percentage	%	87	57	D_R
Reference Effective Confining Pressure	kPa	100	100	P_r'
Reference Low-Strain Shear Modulus	MPa	111.9	73.7	$refShearModul
Poisson's Ratio	-	0.33	0.33	ν
Reference Bulk Modulus to Reference Shear Modulus Ratio	-	2.67	2.67	B_r/G_r
Reference Bulk Modulus	MPa	298.3	196.8	$refBulkModul
Shear Strain at Maximum Shear Strength	-	0.1	0.1	$peakShearStra
Positive Constant Defining Shear/Bulk Modulus Variations	-	0.5	0.5	$pressDependCoe
Internal Friction Angle	degrees	42.2	30.3	$frictionAng
Phase Transformation Angle	degrees	32.2	25.3	$PTAng
Controls Contraction Rate and Pore Oressure Increase	-	0.001	0.019	$contrac1
Controls Compaction Rate	-	0.5	3	$contrac2
Considers Overburden Stress Effects	-	0	0.2	$contrac3
Controls Dilation Rate from Shear Stress	-	0.4	0.15	$dilat1
Controls Dilation Magnitude	-	3	3	$dilat2
Considers Overburden Stress in Dilation	-	0	0	$dilat3
Controls Plastic Shear Strain from Liquefaction	-	1	1	$liquefac1
Secondary Liquefaction Parameter	-	0	0	$liquefac2
Number of Yield Surfaces	-	20	20	$noYieldSurf
Critical State Line Parameter 1	-	0.9	0.9	$cs1
Critical State Line Parameter 2	-	0.02	0.02	$cs2
Critical State Line Parameter 3	-	0	0	$cs3
Atmospheric Pressure	kPa	100	100	$pa
Shear Strength at Zero Confining Pressure	-	0.1	0.1	$c

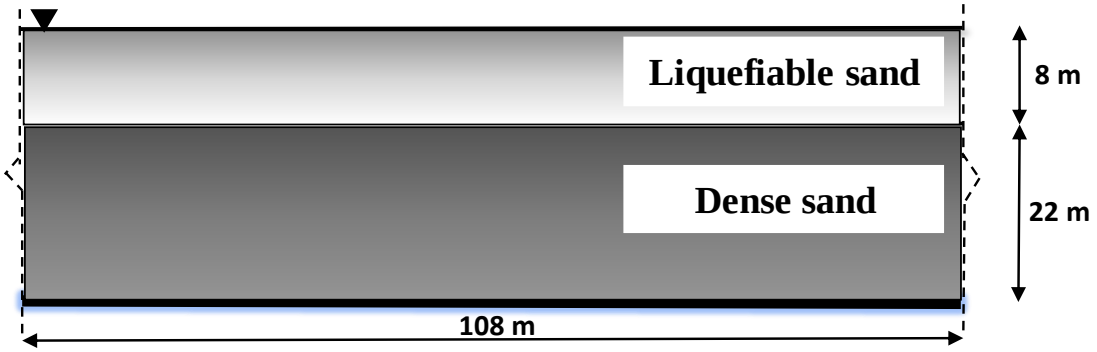

Fig. 20. Graphical representation of soil stratification in the present study.

8. Results and discussion

In this section, the results of soil-pile-structure system analysis under various ground motion records are examined. Since the primary objective of this research is to investigate the seismic behavior of braced frame systems in sandy soils susceptible to the liquefaction phenomenon, different lengths and diameters of pile groups were utilized to consider the liquefaction effects. To be able to study the effects of this phenomenon on the seismic behavior of braced frame structures, all analyses were conducted in two conditions: the presence and absence of the liquefaction phenomenon.

8.1. Roof displacement response

Roof displacement is considered a fundamental parameter in structural design. Generally, the lower the roof displacement, the more beneficial it can be for structural safety. The average roof displacement for the 4-story diagrid structure in two conditions of liquefaction occurrence and its absence is presented in Figure 21. This response represents the average response obtained from seven selected records that were processed and derived using MATLAB software. In the condition where the liquefaction phenomenon does not occur, the soil permeability coefficient was entered as unity and liquefaction parameters as zero in the software. In all figures of this section, condition A represents the state of liquefaction occurrence, and condition B represents the state without liquefaction.

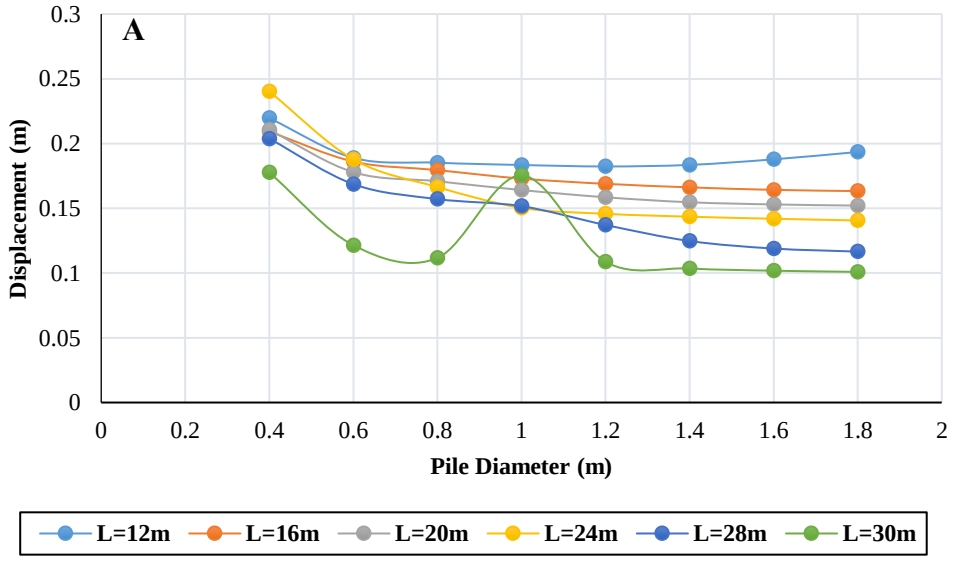

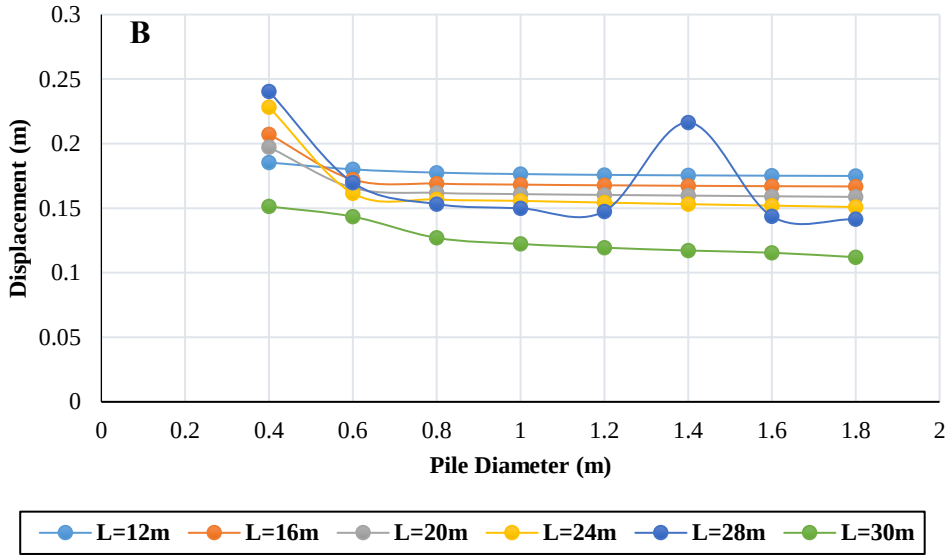

Fig. 21. Average roof displacement of 4-story diagrid structure in two conditions of liquefaction occurrence (A) and its absence (B).

In the liquefaction occurrence condition, roof displacement decreases with increasing pile length. For instance, roof displacement at a 1.8-meter diameter from 12-meter to 30-meter pile length decreases by 50% and 33% for conditions A and B, respectively. In condition A, increasing diameter results in reduced roof displacement. However, displacement of 12-meter piles slightly increases at larger diameters. In condition B, displacement remains constant from 0.6-meter diameter onward. Pile length at 0.4-meter diameter has a different effect on displacement magnitude, such that maximum displacement in condition A occurs for a 24-meter pile length and in condition B for a 28-meter pile length. Displacement jumps are observed in conditions A and B. The observed peak response may be attributed to the proximity between the system's fundamental period (0.31 sec) and the dominant excitation period of the ground motions (0.40 sec), which amplifies structural demands through resonance effects. This relationship reinforces the need to consider spectral alignment in seismic design to mitigate response amplification. The observed increase in roof displacement for 24-meter piles under liquefaction is primarily attributed to an imbalance between pile length and stiffness, compounded by reduced soil support due to liquefaction: 1) Intermediate pile length (24 m) does not fully engage deeper, more stable soil strata, which longer piles (28–30 m) are able to reach. 2) Under liquefaction, the upper soil layers lose stiffness, reducing lateral confinement and increasing pile head flexibility. The 24-meter piles experience larger lateral deflections and rotations, transferring greater displacement to the superstructure. 3) The dynamic soil-structure interaction becomes more pronounced at this pile depth, magnifying inertial forces and leading to elevated roof drift.

8.2. Story drift response

Inter-story drift ratio is considered another important parameter in structural design. This response must be less than the allowable limit in design to ensure good structural resilience against earthquakes. The design was performed for the Life Safety (LS) level, with an allowable drift limit of 1.5% according to the mentioned design code and FEMA 273. For the 4-story structure, according to Figure 22, response amplification similar to displacement response is observed in cases L30D1.0 and L28D1.4, the cause of which was explained. The maximum inter-story drift response of foundations with a 30-meter pile length is inappropriate in all diameters and exceeds the 1.5% limit.

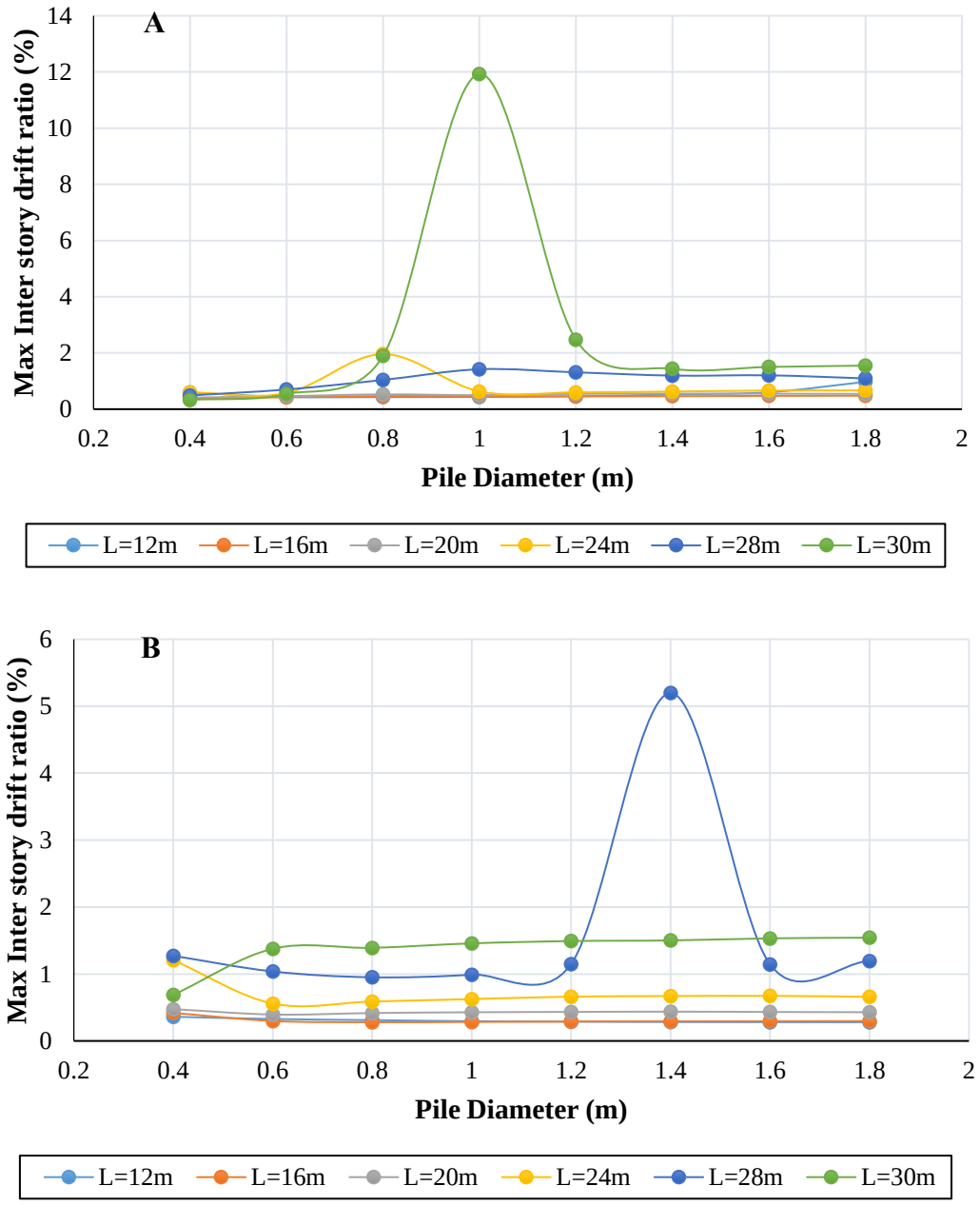

Fig. 22. Average maximum inter-story displacement of 4-story diagrid structure in two conditions of liquefaction occurrence (A) and its absence (B).

In conditions A and B, increasing pile length has increased the inter-story drift magnitude, while diameter increase has not had a significant effect on this response. The lowest response in both conditions corresponds to pile lengths of 12, 16, and 20 meters in all diameters.

8.3. Maximum axial force response

As mentioned, the critical stress for diagonal members of diagrid structures is axial force. Therefore, the average (among 7 selected records) maximum axial force in stories of the 4-story diagrid structure in two conditions of the liquefaction phenomenon occurrence and its absence is shown in Figure 23. Generally, it is observed that with increasing pile length, axial force in diagonal structural members increases, while increasing pile diameter does not have such an effect on the axial force magnitude of structural members. At 0.4-meter diameter, responses are minimal, and this trend is observed in both conditions A and B. Similar to the two previous responses, responses are amplified in cases L28D1.4 and L30D1.0.

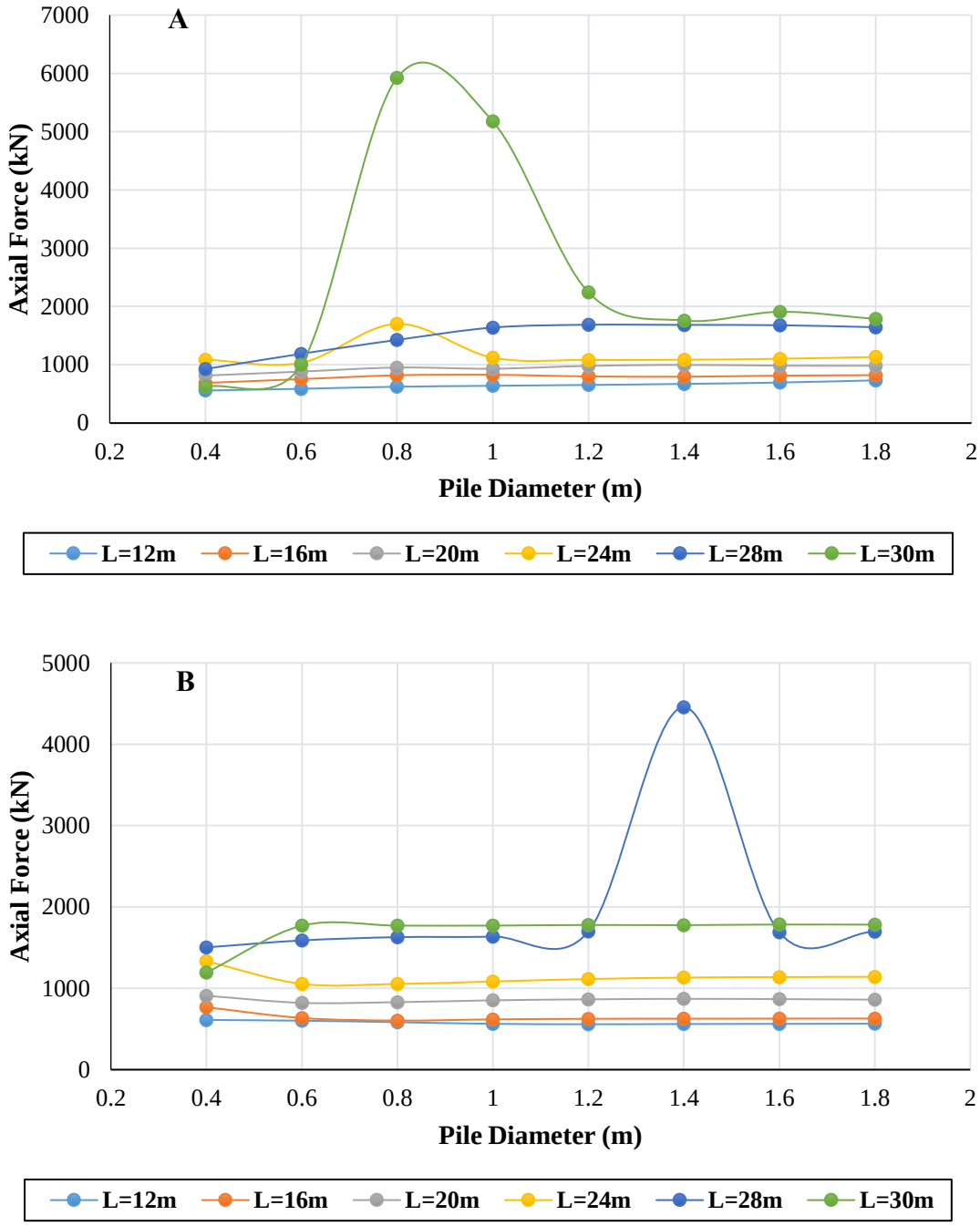

Fig. 23. Average maximum axial force of 4-story diagrid structure in two conditions of liquefaction occurrence (A) and its absence (B).

8.4. Foundation displacement response

The horizontal displacement of the foundation for the 4-story structure in liquefaction condition (A) and non-liquefaction condition (B) is presented in Figure 24. In conditions A and B, with increasing pile length, the horizontal displacement of the foundation decreases. Except for 28- and 30-meter piles, increasing pile diameter does not have a significant effect on foundation displacement. The displacement magnitude varies between 6 to 16 centimeters depending on the case.

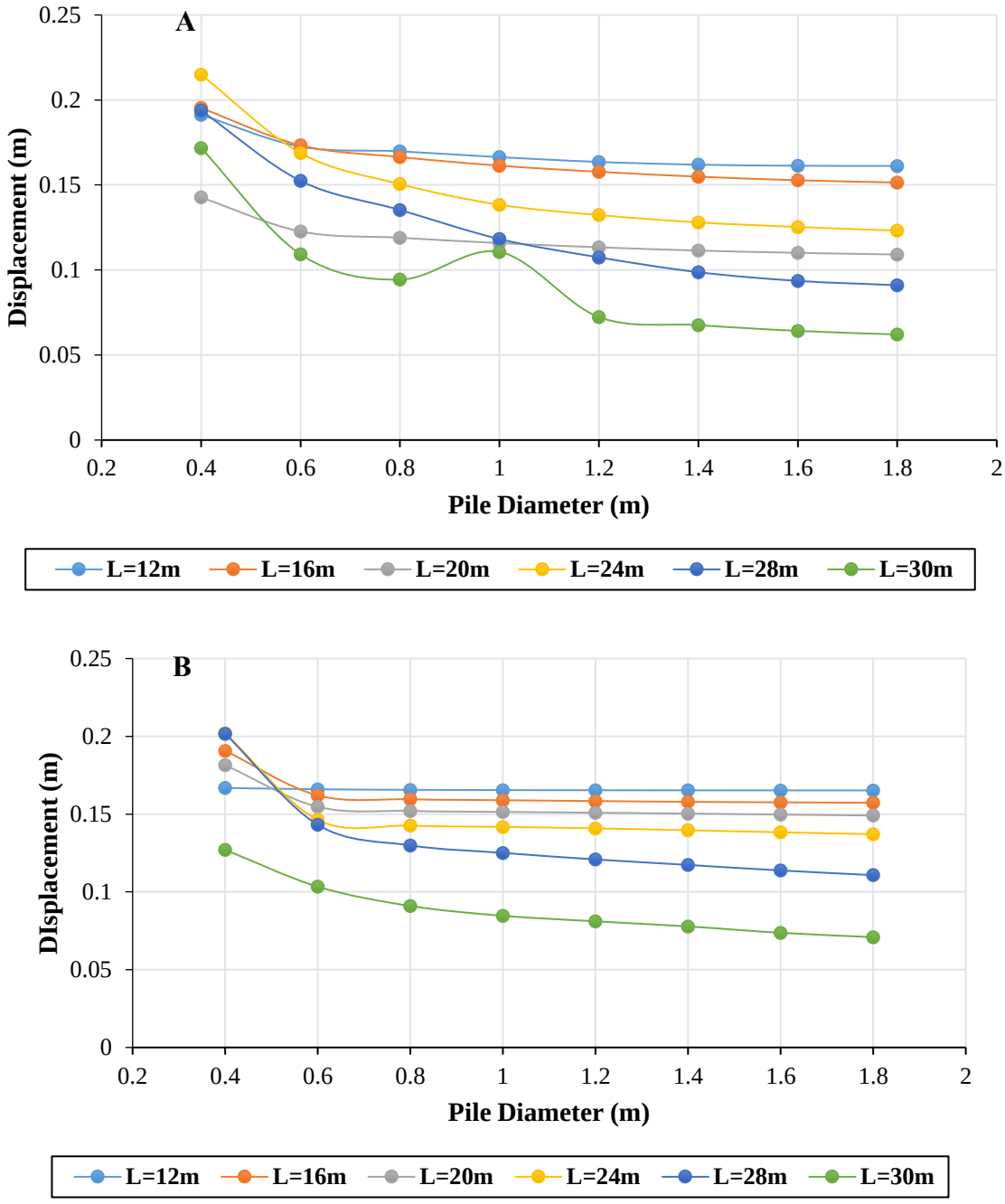

Fig. 24. Average horizontal displacement of foundation for 4-story diagrid structure in two conditions of liquefaction occurrence (A) and its absence (B).

8.5. Foundation rotation response

Figure 25 presents the average foundation rotation of the 4-story diagrid structure in two conditions of liquefaction occurrence (A) and its absence (B). As observed and expected, with decreasing pile length, foundation rotation increases. The rotation of 30-meter piles is naturally approximately zero. However, this rotation must be within its allowable limits, similar to structural drift. The allowable limit of foundation design codes, in cases where cracking occurs in the building (maximum limit), is between 0.002 to 0.0033 radians, and in cases where structural damage exists in the building (ultimate limit), is between 0.004 to 0.0067 radians. The allowable limit for foundation settlement is also considered 5 centimeters for uniform settlement and 2 centimeters for non-uniform settlement.

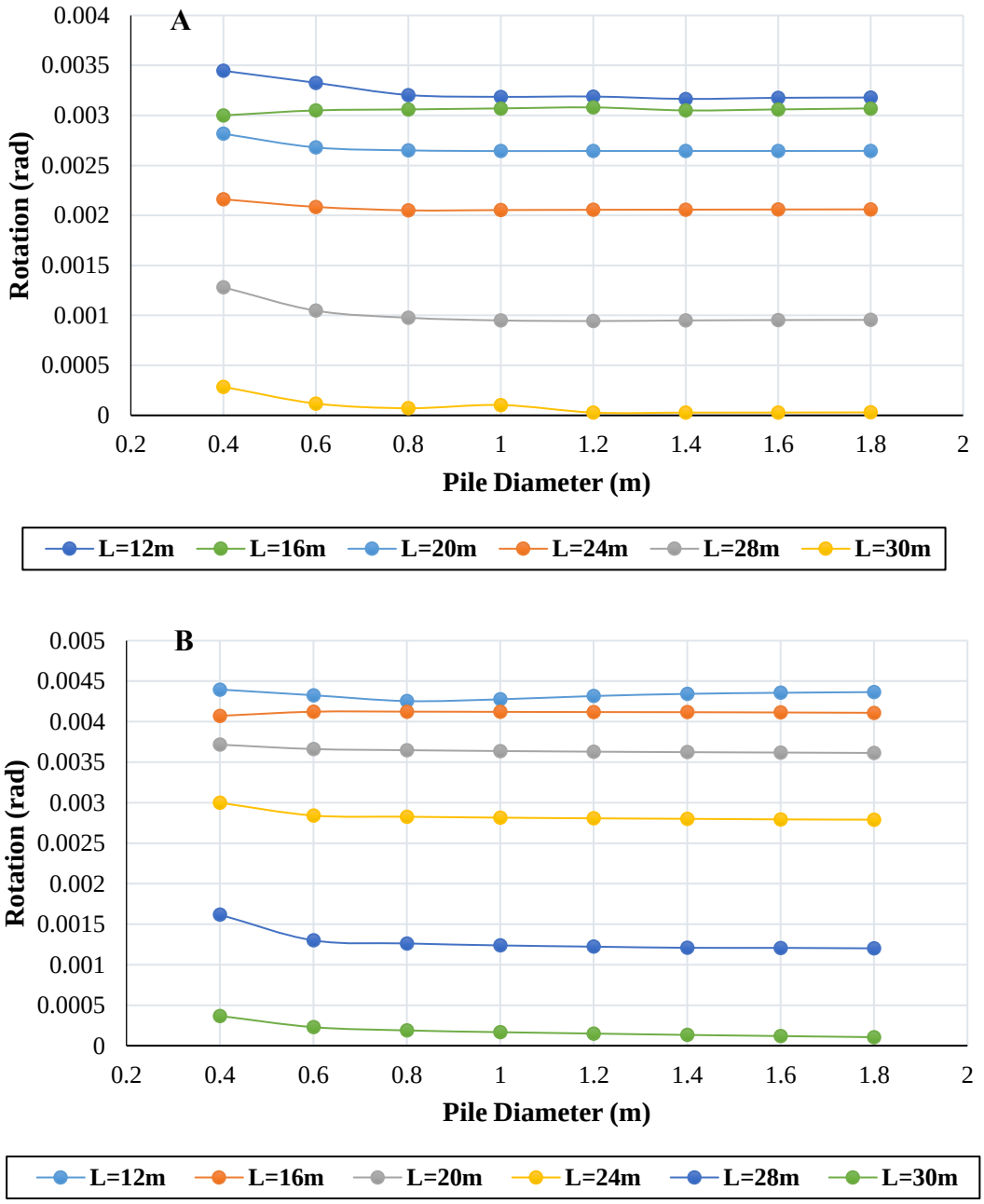

Fig. 25. Average foundation rotation of 4-story diagrid structure in two conditions of liquefaction occurrence (A) and its absence (B).

In cases of 28- and 30-meter piles, foundation rotation is below the maximum limit (0.002). In other existing cases, they fall between the maximum and ultimate limits (0.0067) and are acceptable. Meanwhile, increasing pile diameter has no effect on foundation rotation magnitude, and 12-meter piles exhibit the highest foundation rotation. Therefore, it can be concluded that 12-meter piles utilize more of the horizontal displacement and foundation rotation capacity within allowable limits. Consequently, this contributes to reducing seismic forces in the superstructure, as explained in the discussions presented.

8.6. Pile shear force response

From Figure 26, in both conditions A and B, case L12 is the case with the lowest possible shear force. On the other hand, the shear forces are highest for longer pile lengths, 28 and 30 meters. Generally, the greater the pile length and diameter, the larger the interface between soil and pile (pile perimeter), and in soil-pile interaction, the pile absorbs more force, which is evident in the graphs of Figure 26. In condition

B, where liquefaction occurs, the depth of the liquefiable layer loses its shear resistance. At this depth, since no soil exists, all seismic energy is sustained by the pile. Therefore, in this condition, increased shear force in piles is evident.

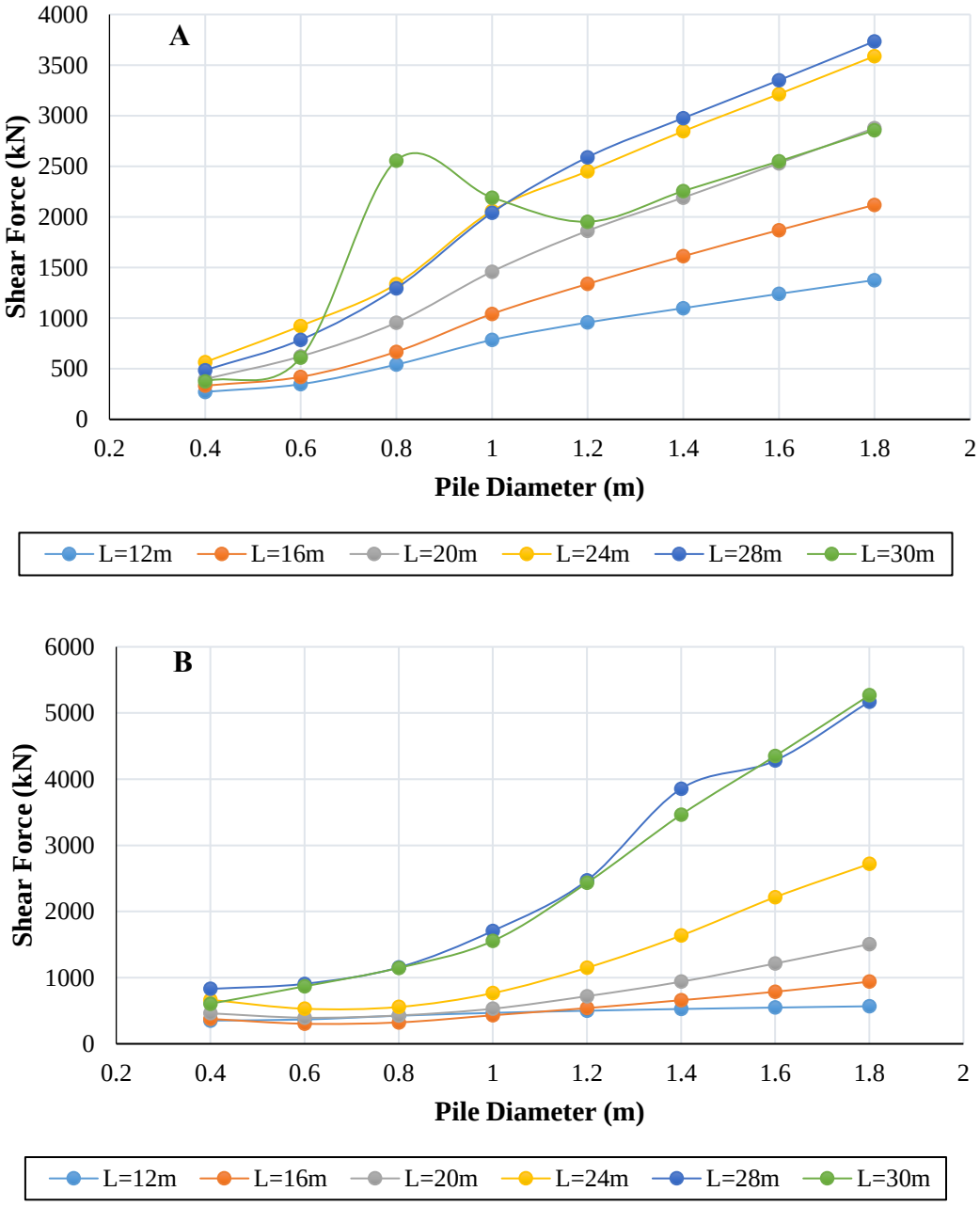

Fig. 26. Average maximum pile shear force in 4-story diagrid structure in two conditions of liquefaction occurrence (A) and its absence (B).

8.7. Pile axial force response

Figure 27 illustrates the average maximum axial force in piles of the 4-story structure in two conditions of the liquefaction phenomenon occurrence (condition A) and its absence (condition B). It is observed that cases L30D1.0 and L28D1.4 also cause amplification of axial force in this type of response. The reason could be the proximity of excitation and structural frequencies. In both conditions, with increasing pile length and diameter, pile axial force increases. The lowest axial force magnitude corresponds to 12-meter piles.

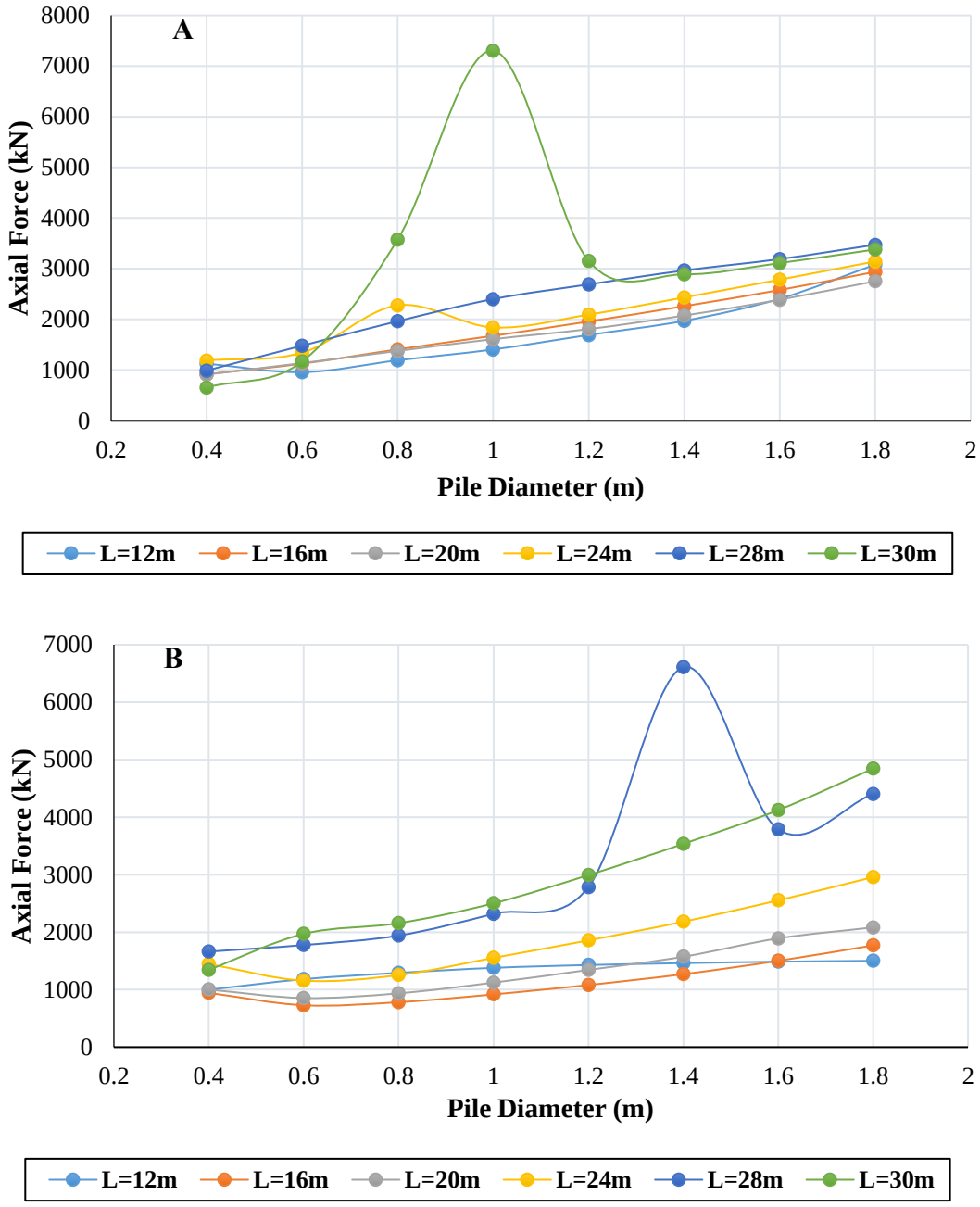

Fig. 27. Average maximum pile axial force in 4-story diagrid structure in two conditions of liquefaction occurrence (A) and its absence (B).

8.8. Pile bending moment response

The average maximum bending moment of piles for the 4-story structure in two conditions of the liquefaction phenomenon occurrence and its absence is presented in Figure 28. It is observed that in the condition of non-liquefaction occurrence, the response of 12-meter piles is not dependent on pile diameter, and with increasing pile diameter, the bending moment magnitude also increases until for 28- and 30-meter piles, the bending moment magnitude is approximately equal across different diameters. For example, at a 1.2-meter diameter, the bending moment in 30-meter piles is approximately 3 times that of 12-meter piles. It is noteworthy that with increasing pile length and diameter, the bending moment also increases.

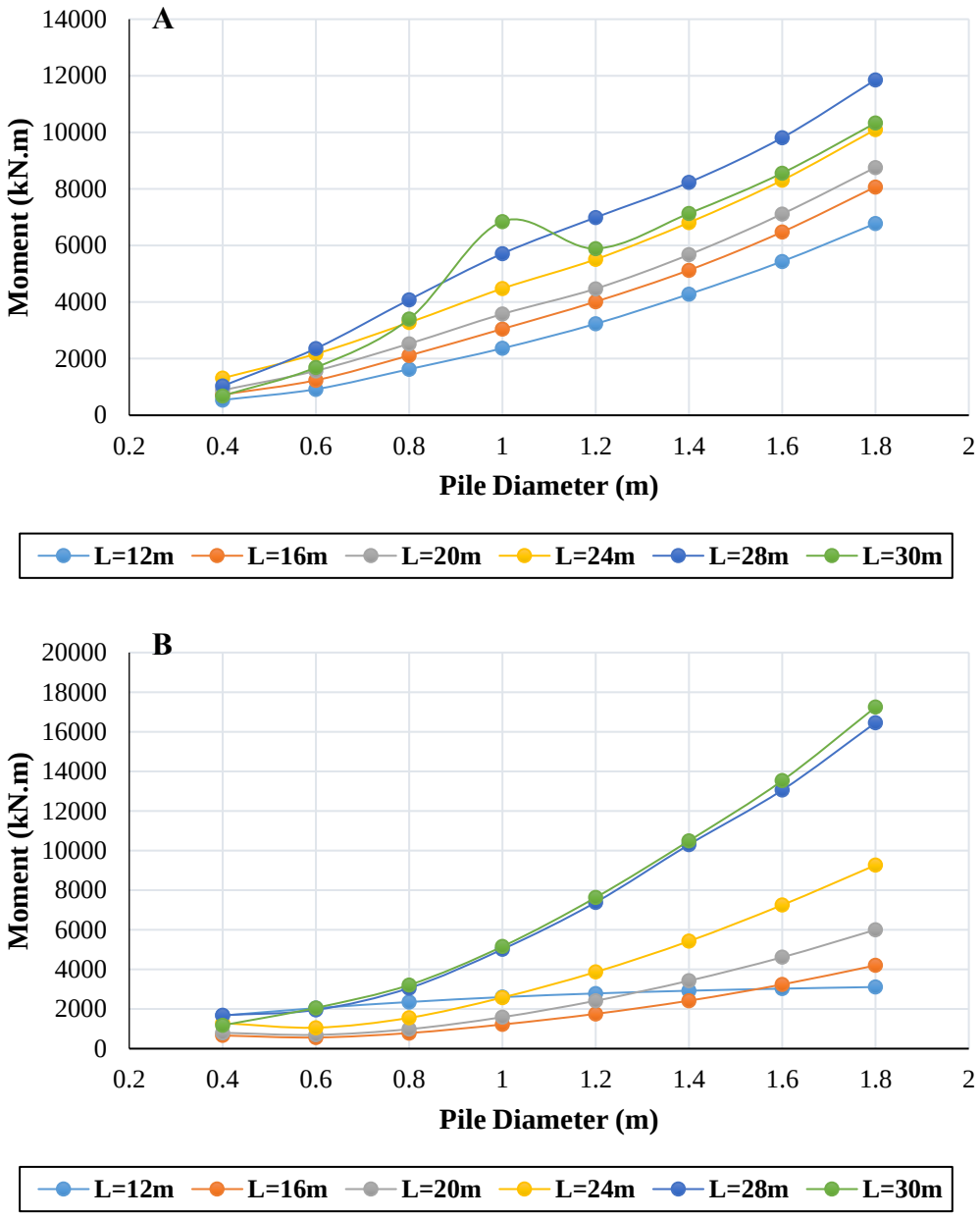

Fig. 28. Average maximum pile bending moment in 4-story diagrid structure in two conditions of liquefaction occurrence (A) and its absence (B).

9. Conclusions

This study investigates the seismic performance of steel diagrid structures in liquefiable sandy soils, focusing on soil-pile-structure interaction effects. A nonlinear model was developed in OpenSees based on a benchmark four-story configuration, incorporating near- and far-field soil domains, piles, and structural components. A suite of seven ground motions was applied to evaluate displacement, drift, and internal force demands.

This study demonstrates that pile length and diameter significantly affect the seismic response of diagrid structures in liquefiable soils. Longer piles (28–30 m) with diameters ≥1.2 m reduce displacement and drift but increase internal stresses. Shorter piles (12 m) mitigate shear and axial force but induce larger displacements—though they show improved drift performance under liquefaction. Increasing diameter beyond 1.2 m yields diminishing returns for displacement control while substantially increasing bending

demands. Frequency coincidence in disproportionate piles further amplifies response. Optimal designs should prioritize moderate diameters with sufficient length and integrate detailed soil-structure interaction analysis. These findings support updating seismic design codes to define pile dimension limits that consider both liquefaction effects and structural performance.

As a suggestion for the design of diagrid buildings located on loose sand with liquefaction potential, it is crucial first to thoroughly understand the soil properties and simulate the designed diagrid buildings along with their foundation system. Following this, a skilled engineer can redesign the diagrid structures by addressing and controlling critical response limitations, such as horizontal and vertical displacements, footing rotation, and pile forces along the soil deposit, especially in regions where the soil undergoes liquefaction. To address these limitations and further advance the field, it is suggested that future work could:

1- Develop 3D numerical models that incorporate full geometric representation of piles and superstructures to better simulate lateral and torsional effects.
2- Investigate pile group interaction effects under liquefaction using more advanced constitutive models and soil layering.
3- Conduct experimental studies and field monitoring to validate model predictions and improve parameter calibration.
4- Explore the effect of non-uniform ground motions and multi-directional excitation, which are particularly relevant for complex urban foundations.

Funding

This research did not receive any specific grant from funding agencies in the public, commercial, or not-for-profit sectors.

Conflicts of interest

The authors declare that they have no known competing financial interests or personal relationships that could have appeared to influence the work reported in this paper.

Authors contribution statement

Ebrahim Mirzaei: Conceptualization, Data curation, Formal analysis, Investigation, Methodology, Resources, Software, Validation, Visualization, Writing – original draft, Writing – review & editing.

Shahriar Tavousi Tafreshi: Conceptualization, Formal analysis, Investigation, Methodology, Project administration, Resources, Supervision, Validation, Writing – original draft, Writing – review & editing.

Farrokh Forootan: Conceptualization, Investigation, Supervision, Writing – review & editing.

References

[1] Motamed R, Sesov V, Towhata I, Anh NT. Experimental Modeling of Large Pile Groups in Sloping Ground Subjected to Liquefaction-Induced Lateral Flow: 1-G Shaking Table Tests. Soils Found 2010;50:261–79. https://doi.org/10.3208/sandf.50.261.

[2] Haeri SM, Kavand A, Rahmani I, Torabi H. Response of a group of piles to liquefaction-induced lateral spreading by large scale shake table testing. Soil Dyn Earthq Eng 2012;38:25–45. https://doi.org/10.1016/j.soildyn.2012.02.002.

[3] Bagheri M, Jamkhaneh ME, Samali B. Effect of Seismic Soil–Pile–Structure Interaction on Mid- and High-Rise Steel Buildings Resting on a Group of Pile Foundations. Int J Geomech 2018;18. https://doi.org/10.1061/(ASCE)GM.1943-5622.0001222.

[4] López Jiménez GA, Dias D, Jenck O. Effect of the soil–pile–structure interaction in seismic analysis: case of liquefiable soils. Acta Geotech 2019;14:1509–25. https://doi.org/10.1007/s11440-018-0746-2.

[5] Brandis A, Kraus I, Petrovčič S. Nonlinear Static Seismic Analysis and Its Application to Shallow Founded Buildings with Soil-Structure Interaction. Buildings 2022;12:2014. https://doi.org/10.3390/buildings12112014.

[6] Mohasseb S, Ghazanfari N, Rostami M, Rostami S. Effect of Soil–Pile–Structure Interaction on Seismic Design of Tall and Massive Buildings Through Case Studies. Transp Infrastruct Geotechnol 2020;7:13–45. https://doi.org/10.1007/s40515-019-00086-7.

[7] Conto Quispe KF. Contributions to dynamic pile-soil interaction modelling. Universitat Politècnica de Catalunya, 2024. https://doi.org/10.5821/dissertation-2117-421132.

[8] Karafagka S, Fotopoulou S, Pitilakis D. The Effect of Soil Liquefaction and Lateral Spreading to the Seismic Vulnerability of RC Frame Buildings Considering SSI. J Earthq Eng 2023;27:4786–808. https://doi.org/10.1080/13632469.2023.2193658.

[9] Castelli F, Grasso S, Lentini V, Sammito MSV. Assessment of liquefaction effects on dynamic soil-structure interaction for the 1908 Messina and Reggio Calabria scenario earthquake. Soil Dyn Earthq Eng 2024;178:108445. https://doi.org/10.1016/j.soildyn.2023.108445.

[10] Hwang Y-W, Dashti S, Tiznado JC. Seismic Interactions Among Multiple Structures on Liquefiable Soils Improved with Ground Densification, 2022, p. 1111–8. https://doi.org/10.1007/978-3-031-11898-2_89.

[11] Vicencio F, Alexander NA, Málaga-Chuquitaype C. Seismic Structure-Soil-Structure Interaction between inelastic structures. Earthq Eng Struct Dyn 2024;53:1446–64. https://doi.org/10.1002/eqe.4076.

[12] Tsutsumi S, Morikiyo N, Tanuma T, Nagano M. Effect Of Dynamic Soil-Pile-Structure-Interaction On Nonlinear Responses Of Super High-Rise Rc Buildings To Pulse-Like Ground Motions. J Struct Constr Eng (Transactions AIJ) 2023;88:722–33. https://doi.org/10.3130/aijs.88.722.

[13] Mazzoni S, McKenna F, Scott MH, Fenves GL. OpenSees command language manual. Pacific Earthq Eng Res Cent 2006;264:137–58.

[14] Prevost JH. A simple plasticity theory for frictional cohesionless soils. Int J Soil Dyn Earthq Eng 1985;4:9–17. https://doi.org/10.1016/0261-7277(85)90030-0.

[15] Elgamal A, Yang Z, Parra E. Computational modeling of cyclic mobility and post-liquefaction site response. Soil Dyn Earthq Eng 2002;22:259–71. https://doi.org/10.1016/S0267-7261(02)00022-2.

[16] Elgamal A, Yang Z, Parra E, Ragheb A. Modeling of cyclic mobility in saturated cohesionless soils. Int J Plast 2003;19:883–905. https://doi.org/10.1016/S0749-6419(02)00010-4.

[17] Khosravifar A, Boulanger RW, Kunnath SK. Effects of Liquefaction on Inelastic Demands on Extended Pile Shafts. Earthq Spectra 2014;30:1749–73. https://doi.org/10.1193/032412EQS105M.

[18] Wilson DW. Soil-pile-superstructure interaction in liquefying sand and soft clay. vol. 1998. University of California, Davis America; 1998.

[19] Institute AP. API RP 2A-WSD: Recommended Practice for Planning, Designing and Constructing Fixed Offshore Platforms — Working Stress Design. Washington, DC: American Petroleum Institute (API Publishing Services); 2000.

[20] Mazzoni S, McKenna F, Scott MH, Fenves GL. Open system for earthquake engineering simulation user command-language manual—OpenSees version 2.0. Pacific Earthq Eng Res Center, Univ California, Berkeley, CA 2009.

[21] GiD the personal pre/postprocessor user's manual. Int Cent Numer Methods Eng (CIMNE),Version 11 ⟨http//GidCimneUpcEs⟩ 2013.

[22] Ilankatharan M, Kutter B. Modeling Input Motion Boundary Conditions for Simulations of Geotechnical Shaking Table Tests. Earthq Spectra 2010;26:349–69. https://doi.org/10.1193/1.3383214.

[23] Khosravifar A, Boulanger RW. Inelastic Response of Extended Pile Shafts in Laterally Spreading Ground during Earthquakes (Student Paper Competition 2010). DFI J - J Deep Found Inst 2010;4:41–53. https://doi.org/10.1179/dfi.2010.009.

[24] Shin H, Arduino P, Kramer SL. Performance-Based Evaluation of Bridges on Liquefiable Soils. Struct. Eng. Res. Front., Reston, VA: American Society of Civil Engineers; 2007, p. 1–16. https://doi.org/10.1061/40944(249)41.

[25] Chiaramonte MM, Arduino P, Lehman DE, Roeder CW. Seismic analyses of conventional and improved marginal wharves. Earthq Eng Struct Dyn 2013;42:1435–50. https://doi.org/10.1002/eqe.2280.

[26] Wair BR, DeJong JT, Shantz T. Guidelines for estimation of shear wave velocity profiles. PEER Report 2012/08, Pacific Earthquake Engineering Research Center. Univ California, Berkeley, USA 2012.

[27] Romney KT. Soil-bridge interaction during long-duration earthquake motions 2013.

[28] Heshmati M, Aghakouchak AA. Quantification of seismic performance factors of steel diagrid system. Struct Des Tall Spec Build 2019;28. https://doi.org/10.1002/tal.1572.

[29] Minimum design loads and associated criteria for buildings and other structures. 2017. https://doi.org/10.1061/9780784414248.

[30] AISC 341-10 - American Institute of Steel Construction. Seismic Provisions for Structural Steel Buildings. 2010.

[31] Construction AI of S. Specification for structural steel buildings. ANSI/AISC 2005;36010.

[32] BHRC Publication. Iranian Code of Practice for Seismic Resistant Design of Buildings (Standard No. 2800). 2016.

[33] Fox PJ. State of the Journal. J Geotech Geoenvironmental Eng 2015;141. https://doi.org/10.1061/(ASCE)GT.1943-5606.0001367.